AD_____

Award Number: DAMD17-02-1-0106

TITLE: Non-Invasive Diagnosis of Androgen Sensitivity in Human Prostate Tumors

PRINCIPAL INVESTIGATOR: Laurel O. Sillerud, Ph.D.

CONTRACTING ORGANIZATION: University of New Mexico Health Science Center
Albuquerque, New Mexico 87131-5041

REPORT DATE: February 2004

TYPE OF REPORT: Annual

PREPARED FOR: U.S. Army Medical Research and Materiel Command
Fort Detrick, Maryland 21702-5012

REPORT DOCUMENTATION PAGE

Form Approved
OMB No. 074-0188

1. AGENCY USE ONLY (Leave blank)	2. REPORT DATE	3. REPORT TYPE AND DATES COVERED
	February 2004	Annual (15 Jan 2003 - 14 Jan 2004)

4. TITLE AND SUBTITLE
Non-Invasive Diagnosis of Androgen Sensitivity in Human Prostate Tumors

5. FUNDING NUMBERS
DAMD17-02-1-0106

6. AUTHOR(S)
Laurel O. Sillerud, Ph.D.

7. PERFORMING ORGANIZATION NAME(S) AND ADDRESS(ES)
University of New Mexico Health Science Center
Albuquerque, New Mexico 87131-5041

E-Mail: laurel@unm.edu

8. PERFORMING ORGANIZATION REPORT NUMBER

9. SPONSORING / MONITORING AGENCY NAME(S) AND ADDRESS(ES)
U.S. Army Medical Research and Materiel Command
Fort Detrick, Maryland 21702-5012

10. SPONSORING / MONITORING AGENCY REPORT NUMBER

11. SUPPLEMENTARY NOTES
Original contains color plates: All DTIC reproductions will be in black and white.

12a. DISTRIBUTION / AVAILABILITY STATEMENT
Approved for Public Release; Distribution Unlimited

12b. DISTRIBUTION CODE

13. ABSTRACT (Maximum 200 Words)
We characterized human prostate tumors by histology and quantitative NMR spectroscopy to determine if altered prostate gene expression produced NMR detectable changes in several metabolites (e.g., citrate, traicylglycerols, taurine, tyronsine). These may provide sensitive and specific predictors of the presence, and the androgen sensitivity, of prostatic adenocarcinoma. Our investigations provided a sound biochemical basis for the application of non invasive, in vivo NMR spectroscopy to assess tumor differentiation and androgen sensitivity in prostate cancer patients. We established a conventional tissue diagnosis by optical histology and computer-aided measurement of epithelial area, on the NMR tissue samples, assigned a Cleason score to each sample, and performed in vitro quantitative 1H and 13C NMR spectroscopic measurements of the metabolic markers on tissue samples form human prostate tumors and adjacent non tumor tissue. Computer based Linear Discriminant Analysis will be used to develop a discrimination function based on the NMR spectroscopic measurements, the histology, Gleason score, and PSA measurements, and the patient's progress, to determine the most specific and sensitive NMR spectroscopic predictors of tumor diagnosis, grade, and hormonal sensitivity. We then applied NMR spectroscopy to human patients to measure the metabolites determined above as the most sensitive and specific predictors of grade, stage, and hormonal responsiveness, and will compare the measurements with patient outcomes.

14. SUBJECT TERMS
No Subject Terms Provided.

15. NUMBER OF PAGES
37

16. PRICE CODE

17. SECURITY CLASSIFICATION OF REPORT	18. SECURITY CLASSIFICATION OF THIS PAGE	19. SECURITY CLASSIFICATION OF ABSTRACT	20. LIMITATION OF ABSTRACT
Unclassified	Unclassified	Unclassified	Unlimited

Table of Contents

Cover..... 1

SF 298..... 2

Introduction.....4

Body.....4

Key Research Accomplishments.....33

Reportable Outcomes.....34

Conclusions.....35

References.....36

Appendices.....37

DOD Prostate cancer program Annual report.

Project Title: " Non-Invasive Diagnosis of Androgen Sensitivity in Human Prostate Tumors "

Principal Investigator: Laurel O. Sillerud, Ph.D.

Introduction

Prostatic adenocarcinoma is expected to be diagnosed in more than 140,000 American men in 2004, leading to more than 35,000 deaths. In order to enhance the survival of these cancer patients new methods for tumor diagnosis and characterization are urgently required. This work seeks to develop a foundation for new methods for tumor characterization through quantitative, nuclear magnetic resonance (NMR) spectroscopy of prostate tissue *in vitro* and the human prostate *in vivo*. This research is particularly timely and important because the results can be rapidly transferred to other institutions due to the widespread availability of suitable clinical MRI instruments. The scientific basis for this research rests on the fact that the metabolism of the normal, highly-differentiated, prostate is unique among bodily tissues in that it maintains, and secretes, large amounts of intermediary compounds, like citrate. This normal metabolism is observable by means of NMR spectroscopy, both *in vitro* and *in vivo*. Tumorigenesis in the prostate occurs with dedifferentiation and profound metabolic changes which again are observable with NMR. Our preliminary results have shown that qualitative NMR spectroscopy can not only distinguish malignant from non-malignant prostate tissue, but that it can also answer the very important clinical question of whether or not a given prostate tumor is androgen sensitive. In particular, NMR detectable metabolites such as citrate, and triacylglycerols may serve to differentiate tumor from benign tissue, while taurine and tyrosine may serve as indicators of the androgen sensitivity of tumors. It remains to be determined, however, which quantitative NMR metabolite measurements provide the most specific and sensitive predictors of malignancy and androgen sensitivity in human prostatic tissue.

Body

We proposed a series of related histological, NMR spectroscopic, and computer-based analyses of human prostate tumor tissue *in vitro* and *in vivo*. Since this is the second funding year, our primary focus has been on performing quantitative ^{13}C NMR spectroscopy on the acquired human prostate tissue samples and on an acquired series of rat tumors which vary in their degrees of differentiation, metastatic potential, and androgen sensitivity. We have also developed and performed quantitative ^{1}H NMR spectroscopy on a number of human patients, including controls of various ages, and patients undergoing vasectomy, treatment with finasteride, and patients bearing frank tumors prior to surgery or biopsy.

A. Histology.

We have performed optical histology on surgical resections of human prostate tissue. The first emphasis was on the use of standard Hematoxylin and Eosin stains. . Prostatic adenocarcinomas are given a histologic grade (Gleason's grading system is used most often, and includes a score of 1 to 5 for the most prominent component added to a score of 1 to 5 for the next most common pattern). Figure 1 shows representative, low magnification views of H&E-stained sections of normal (left) and Gleason grade 9 (right) human prostate tumors. The normal glandular architecture is visible on the left, with well-isolated acini embedded within dense stroma. The glandular lumens are clear and there is only moderate hypertrophy of the epithelial elements in a portion of the acini, with loss of intervening stroma. The adenocarcinoma sample on the right was given a Gleason grade of 4+5=9. The glandular lumens have been filled with neoplastic tumor cells in most cases, but some lumens have simply lost their epithelium and only retain their basement membrane. There is also infiltration of the stroma by tumor cells. We assigned a Gleason score to each tumor sample.

Figure 1. Hematoxylin and Eosin stained sections of human prostate tissue samples. Normal (left) and Gleason grade 9 (right) tumor tissues.

The normal histologic appearance of prostate glands and surrounding fibromuscular stroma is shown at high magnification in Fig. 2 (left). The normal prostate tissue on the left shows well-differentiated glands lined with tall columnar epithelial cells. The nuclei are located at the bases of the epithelial cells, next to the prominent basement membrane. These cells do not have prominent nucleoli or mitotic figures. On the right is prostatic adenocarcinoma. Note how the glands of the carcinoma are completely filled with tumor cells evidently derived from the epithelium. This tumor sample shows prominent nucleoli and mitotic figures. The stroma appears relatively normal, except for the areas of tumor invasion.

We used computer-aided measurements of epithelial area in these sections to derive values for the relative amounts of epithelium in normal and malignant samples. Normal prostate contains modest amounts of epithelium; the average is 12.7 ± 5.9 % by area. Prostatic adenocarcinoma, on the other

hand contains twice the epithelium at 25.3 ± 7.9 % by area. This is a clear reflection of the fact that most prostatic adenocarcinoma cells have an epithelial origin.

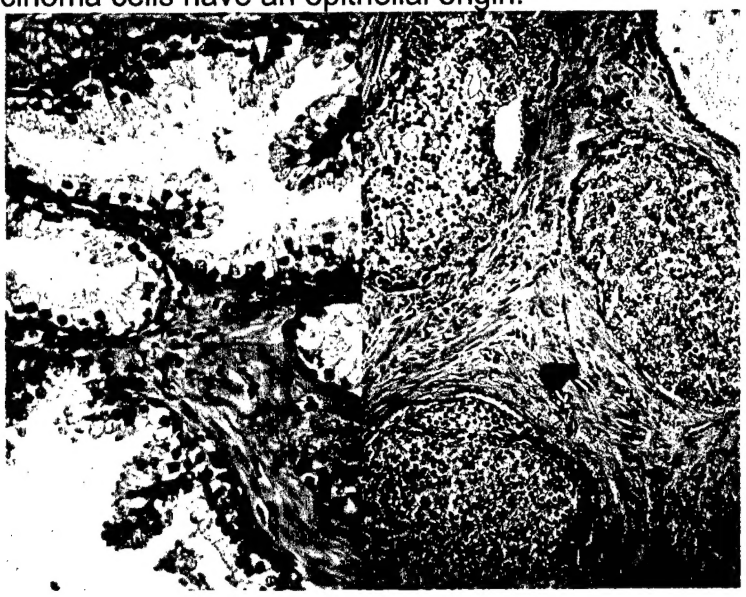

Figure 2. High-magnification photomicrographs of Hematoxylin and Eosin stained sections of human prostate adenocarcinoma samples. Normal (left) and Gleason grade 9 (right) tumor tissues.

Our next task will be to utilize special stains (Oil Red O, Prostate Specific Antigen, Prostatic Acid Phosphatase) to reveal additional tissue characteristics for adenocarcinoma compared with normal controls. Our hypothesis is that the increased lipids found in prostate adenocarcinoma samples will be observable with the aid of lipid-specific stains, such as Oil Red O. We also expect that the alteration in gene expression which results in tumorigenesis will lead to enhanced staining for Prostate Specific Antigen, and perhaps Prostatic Acid Phosphatase. We will develop antibody-based staining techniques (commercially available) for these antigens as well.

B. *In vitro* quantitative ^{13}C NMR spectroscopy.

Our task here was to develop quantitative one-dimensional ^{13}C NMR spectroscopy for the non-destructive measurement of metabolites in human tissue samples from resected prostates. This required us to perform calibration of the NMR standards and pulse sequences. As an example of the work performed along these lines, we use our calibration of the citrate ^{13}C NMR signals. The observation of metabolite signals in the NMR spectrum of a mixture is not necessarily quantitative unless attention is paid to several, well-known features of NMR spectroscopy. (1) The NMR signals are acquired using signal averaging in which multiple samplings of the free induction decay (FID) from the sample are coherently added in the spectrometer computer memory. These samplings are repeated as often as is practical (2-3 per second) in order to build up adequate signal to noise for the FID. The nuclear magnetization does not return to thermal equilibrium under these conditions because the NMR relaxation times are on the order of 1-2 seconds. Therefore, the NMR relaxation times must be measured and the data must then be corrected for this partial saturation of the NMR signals. Fortunately, this correction is easily measured and applied. For example, we measured the NMR relaxation time for the 2,5 carbons of citrate to be 1.6 seconds in physiological saline at pH 7.4.

(2) The strength of ^{13}C NMR signals can be increased by a factor of up to 3, or the time required to reach a given signal to noise ratio can be cut by about a factor of 10 if one utilizes the nuclear Overhauser enhancement (NOE) obtained through proton decoupling during carbon FID acquisition. Thus, the $\{^1H\}$-^{13}C NOE must be measured in order to correct the ^{13}C signal integrals for the enhancement factors. For small molecules in solution the NOE is 2.998. We have measured the NOE for citrate and found it to be 3.0 ± 0.1, in agreement with expectations. (3) One must know the number of carbon nuclei which give rise to a given peak, and correct for this multiplicity. For the citrate, δ = 45 ppm signal, 2 carbons contribute (C2 and C5). (4) Finally, the NMR signal is proportional to the number of nuclei within the detector coil, but the constant of proportionality is unknown. We can correct for this by measuring the NMR signal from a known number of nuclei by using an internal standard present in all of the sample acquisitions. A 1 mm capillary intensity and chemical shift standard containing 10 µl CrAcAc-doped-acetonitrile (δ = 5 and 121 ppm) was used (Fig. 3). The determined citrate amount was also normalized to a standard tissue weight (1.0 gram). Representative control and tumor ^{13}C NMR spectra are shown in Fig. 5 (below).

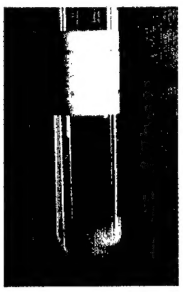

Figure 3. A human prostate tumor sample contained within a glass NMR tube. The black central rod is a fiber-optic thermometer probe for monitoring the sample temperature in real-time. The tumor sample is visible as the pink tissue at the bottom of the tube. The reference capillary containing 10 µl CrAcAc-doped-acetonitrile is visible to the left of the thermometer probe. The white plug at the top of the sample is teflon which serves to hold the thermometer and capillary in place during the measurement.

In order to calibrate the NMR measurements, the amount of citrate in a given tumor tissue sample was determined in two separate ways (1) by means of a citrate assay using a commercial product supplied by Boerhinger-Mannheim, and (2) by means of ^{13}C NMR spectroscopy combined with the above mentioned data correction factors. A correlation plot of the data obtained is shown as Fig. 4, where one notes that the NMR-determined citrate values agree with those found using the enzymatic assay. The slope of the least-squares line fitted to the data was 1.06 ± 0.10 (which is not significantly different from 1.0) with an r^2 = 0.91. The intercept was not significantly different from zero (-0.54 ± 0.76). These data indicate that all of the citrate in tumor tissue is visible to NMR and that the NMR method provides accurate quantitation of tumor metabolites.

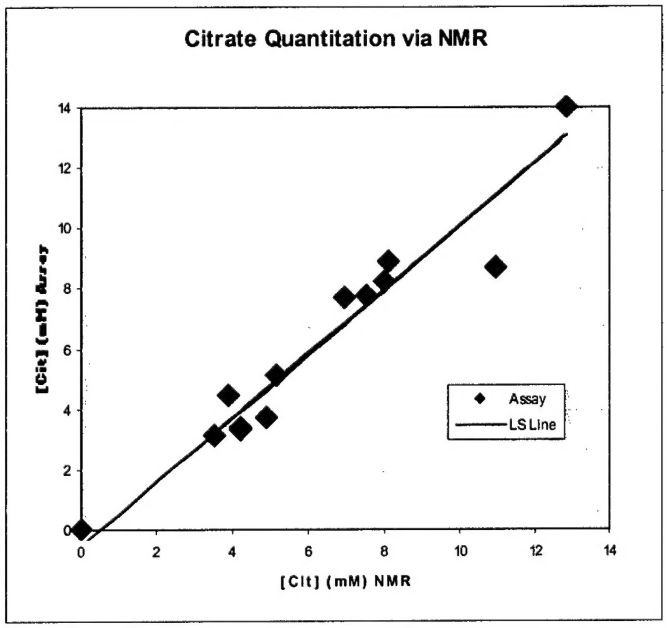

Figure 4. Relationship between prostate tissue citrate concentrations determined by means of an enzymatic citrate assay and ^{13}C NMR Spectroscopy. The line is a least-squares fit to the data with a slope of 1.06 ± 0.10 and r^2 = 0.91.

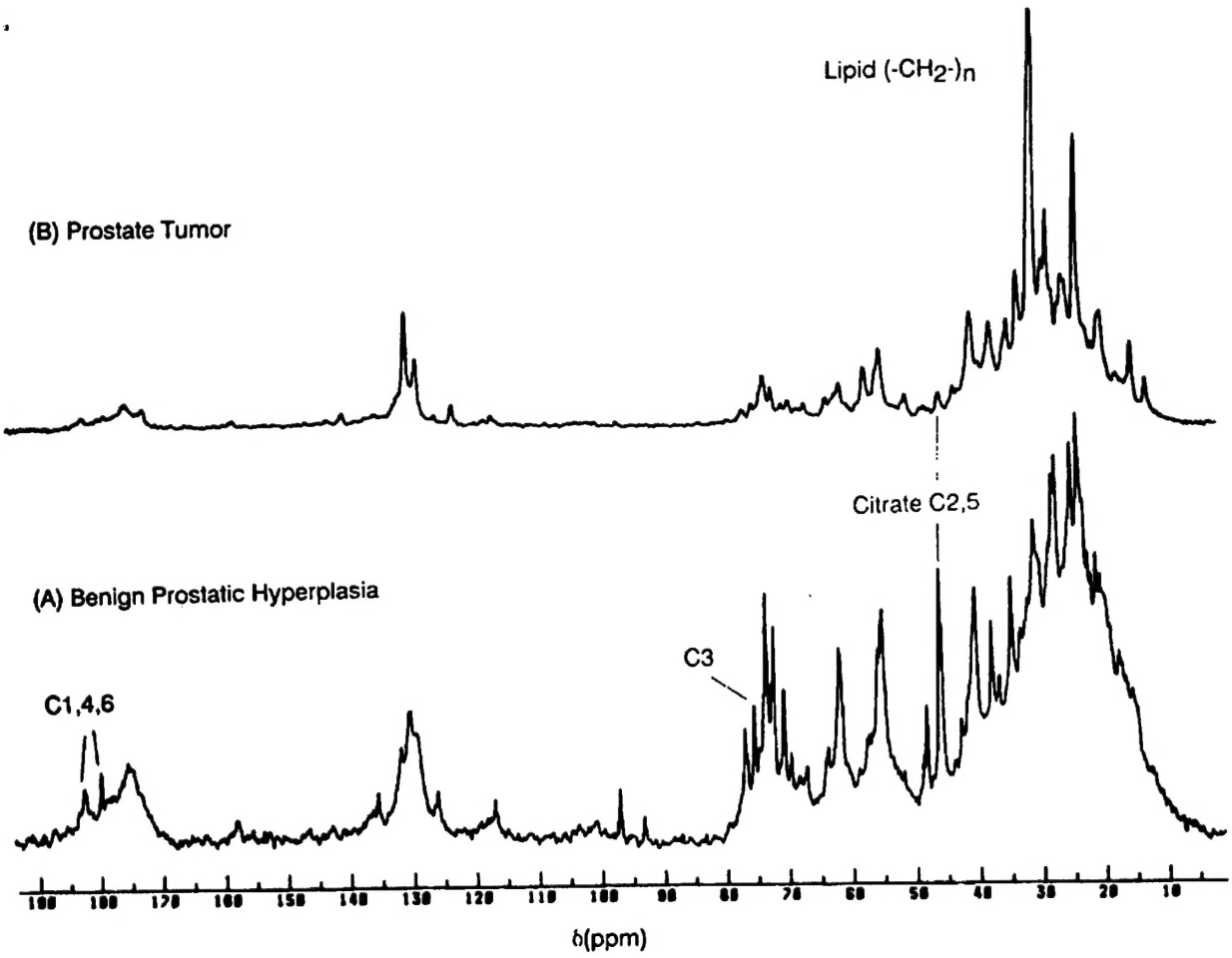

Figure 5. Natural abundance, proton-decoupled ^{13}C NMR spectra at 100.61 MHz of (A) non-malignant benign hyperplastic prostate tissue, and (B) prostate tumor tissue. Indicated are the resonances from citrate (C2,5; C3; and C1,4,6) and from the methylene $(-CH_2-)_n$ carbons. A 22.5 kHz sweep was accumulated in 16,384 data points in an acquisition time of 0.326 s following a 90° pulse. The pulse repetition rate was 0.94/sec. In order to minimize sample heating, a bilevel WALTZ-16 decoupling scheme was used with a power level of 1 Watt applied during the acquisition time and a level of 0.4 Watt applied during the interpulse delay.

^{13}C NMR of non-malignant human prostate tissue.

We next turned to the measurement of a number of metabolites in prostate tissue samples by means of ^{13}C NMR spectroscopy. The results (Fig. 5A) show that we can observe, natural-abundance ^{13}C NMR spectra from tissue samples obtained from residual human prostate tissue obtained during surgical resection of the gland. Signals from citrate carbons $C_{2,5}$ and lipid methylene carbons $(-CH_2-)_n$ were resolved well-enough so that measurements could be made of their respective intensities. Quantitative agreement was found between the citrate integrals (at δ = 47 ppm), relative to the standard, and the results of an enzymatic assay performed on the tissue after the NMR studies were completed (see above).

^{13}C NMR of malignant human prostate tissue.

A Natural-abundance ^{13}C NMR spectrum of a sample of human prostate tumor (Fig. 5B) shows that the citrate signal in the tumor is markedly smaller, while the lipid methylene signal (at 30.5 ppm, Fig. 3B) is much larger than that seen in the normal tissue. Other resonances arise from lactate (20.9 ppm) and inositol (near 74 ppm).

Citrate and lipids in nonmalignant vs malignant prostate.

The citrate $C_{2,5}$ (δ = 47 ppm) and lipid methylene $(-CH_2-)_n$ (δ = 30.5 ppm) carbon peak heights were measured and corrected for differences in sample weights, by normalization to the signal intensity per gram of tissue with respect to the intensity of the standard. The data were pooled into tumor (n=10) and non-malignant (n=24) groups based on the histologic diagnosis. Overall, the data (Fig. 6) confirmed that citrate amounts are higher and lipid amounts are lower in benign tissue in comparison to malignant tissue. The difference in normalized citrate peak intensity between benign and malignant human prostatic tissue was found to be statistically significant by Student's t-test for unequal variances ($p < 0.02$). There is overlap between the two groups, however, because citrate levels alone are unable to discriminate between low citrate tumors and low citrate stromal hyperplasia. Comparison of the lipid methylene peak intensities revealed that lipid differences between benign and malignant tissue values are even more significant ($p < 0.005$), and with less overlap.

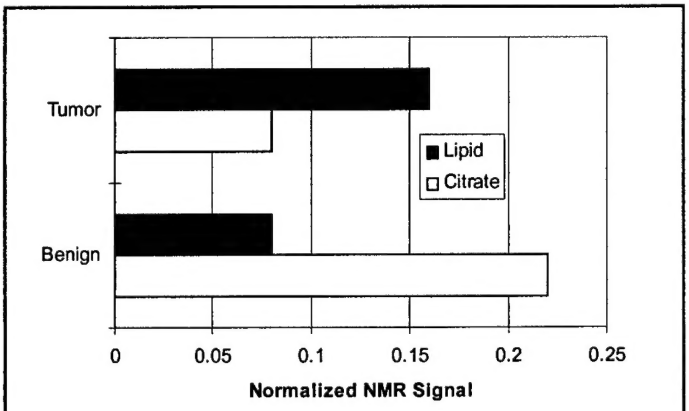

Figure 6. Citrate and lipid (triacylglycerol) results from ^{13}C NMR spectroscopy of 34 human prostate samples.

Correlation of citrate amounts with prostatic epithelial area.

The prostate is an exocrine gland which normally secretes a mixture of citrate and other compounds into seminal plasma. The secretory component of the tissue is presumably the epithelium which lines the acini. We sought to determine if histological data derived from our inital sample of tissues was congruent with our NMR results. We determined the amount of epithelium (expressed as a percentage of the total measured area) of our samples by using optical stereology of the stained tissue sections. The NMR results were obtained from the sample of 34 specimens mentioned above. The results showed that there was a direct correlation between the epithelial area and citrate production (Fig. 7) in the benign samples. The slope of the linear fit to the data is significantly different from zero ($p < 0.001$). It is interesting to note that the fitted line passes through the origin, implying that we were correct in our assumption that epithelium alone produces citrate. On the other hand, the results for the malignant samples (Fig. 7) show a weak inverse correlation between citrate and epithelial area. This is to be expected if our hypothesis about the lack of citrate production in tumors is correct. Note that the tumors have large areas of epithelium and low amounts of citrate. At high amounts of epithelium, most of the epithelial tissue is malignant. Presumably the citrate produced in tumors comes predominantly from the areas of nonmalignant epitheliun, and that is why the fitted line has a negative slope.

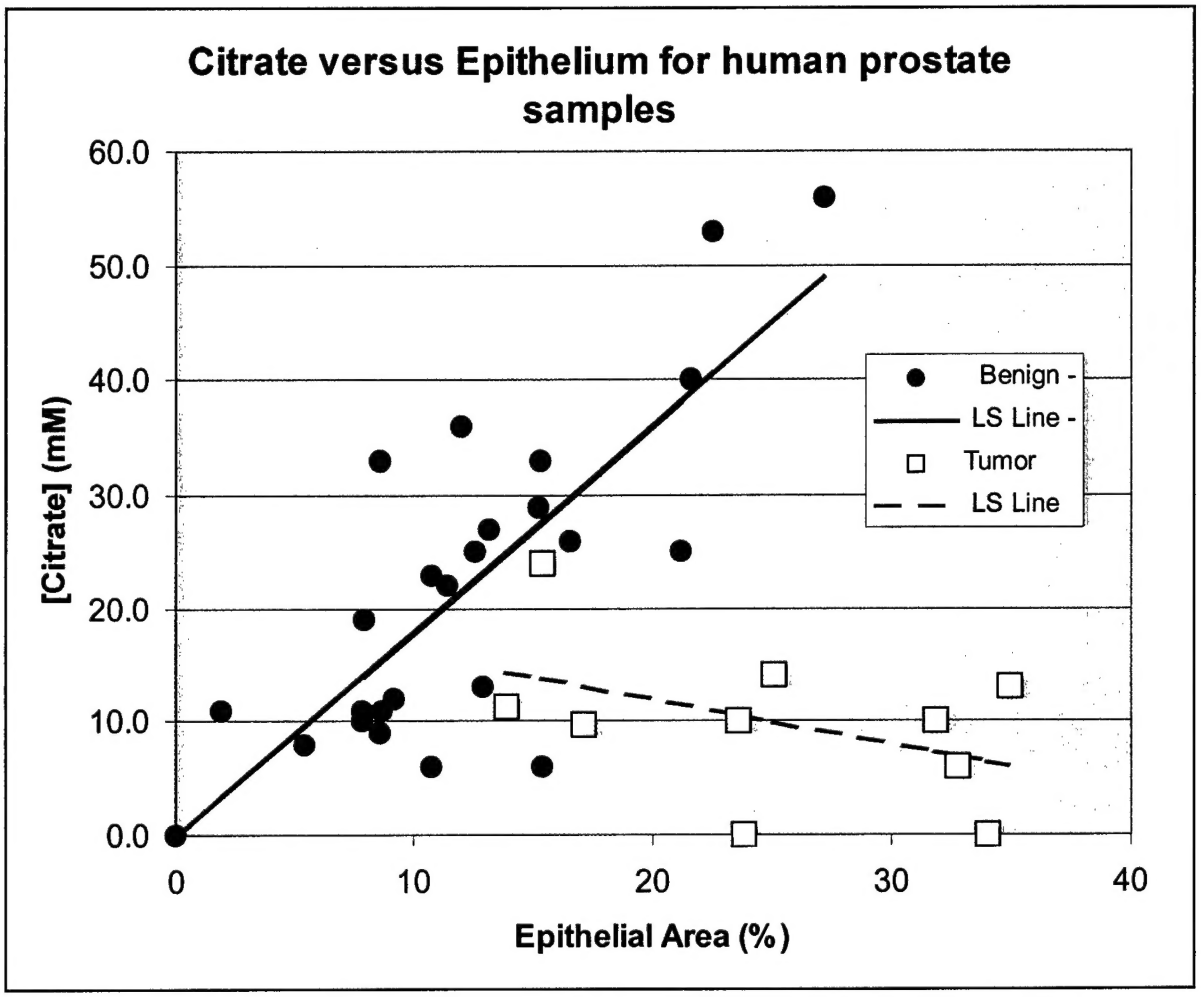

Figure 7. Relationship between the concentration of citrate determined by means of quantitative ^{13}C NMR spectroscopy and the amount of epthelium in H&E stained sections determined by area analysis of the same human prostatic adenocarcinoma tissues.

2.C.1. ^{13}C NMR spectroscopy of excised Dunning rat prostate tumors. The question of the hormonal sensitivity of prostate tumors is one of great clinical significance, but it is also virtually impossible to address in retrospective human studies. In order to study metabolic features which may differ on the basis of androgen response it is necessary to utilize a model system with consistent and well-established characteristics. The Dunning rat model is the most extensively studied of the prostate tumor models (*Claflin et al., 1977*). The original Dunning rat prostatic 3327H tumor was a spontaneous adenocarcinoma of the dorsolateral prostate in an aging Copenhagen rat (*Dunning 1963*). Several tumor lines derived from the original 3327H tumor now exist which resemble human prostatic adenocarcinoma (*Dunning 1963; Claflin et al., 1977; Hall et al., 1985*). These lines include the G, HI, AT-1, ML, and MLL cell types, each of which differs in its Androgen sensitivity, metastatic potential and degree of differentiation (Table 1). Excised rat tumor tissue was obtained from Don Mickey (*Mickey et al., 1977*) at the University of North Carolina. Fresh tissues were immediately frozen in liquid nitrogen and shipped to us on dry ice. Natural abundance ^{13}C NMR spectra were obtained from tumor samples (0.9 to 5.0 g) at 10 °C at 100.6 MHz. The prostatic tissues and tumors examined are shown in Table 1.

Table 1. ***Characteristics of Dunning Rat Prostatic Tissues and Tumor Types Examined with ^{13}C NMR Spectroscopy.***

Tissue or Tumor Type	Androgen Sensitivity	Degree of Differentiation	Metastatic Potential
Normal dorsolateral prostate	Yes	Well	None
Normal ventral prostate	Yes	Well	None
G cell line	Yes	Poor	None
HI cell line	No	Well	None
AT-1 cell line	No	Poor	None
ML cell line	No	Poor	Yes
MLL cell line	No	Poor	Yes

2.C.2. The *in vitro* natural abundance ^{13}C NMR spectra of the rat ventral prostate (Fig. 8) shows at least 51 signals which can be assigned to 27 different metabolites. The assignment process involved the examination of the chemical shifts, linewidths and multiplicity of the signals from each putative compound. We also included an external intensity standard consisting of a 1 mm capillary

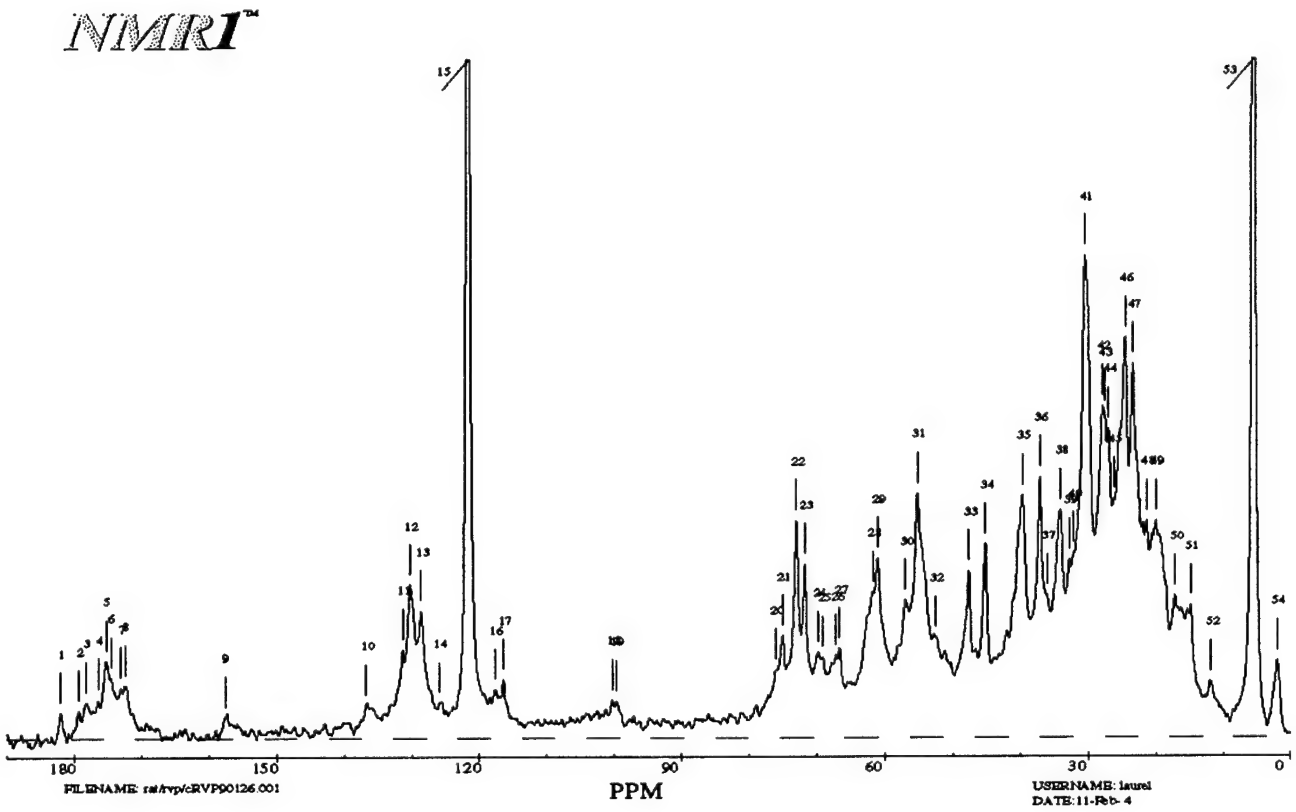

Figure 8. Natural abundance ^{13}C NMR spectrum of 0.5 gram of rat normal ventral prostate tissue. The signals numbered 15 and 53 arise from the acetonitrile external reference in a capillary. Note citrate (peak 34) at 45 ppm, and the small lipid signal at 30.5 ppm (peak 41).

containing 10 μl of chromium-acetylacetonate doped acetonitrile. This could not be used as a chemical shift standard, however, because the paramagnetic Cr introduced concentration-dependent chemical shift changes in the acetonitrile resonance frequencies. The main effect of the Cr was to markedly shorten the acetonitrile T_1 so that we could use the integrals of the acetonitrile signals as an intensity standard. The Cr also quenched the acetonitrile nuclear Overhauser effect so that the integrals of the CN carbon were identical to those from the $-CH_3$ carbon, even though the latter carbon was protonated and could have given rise to a full 2.998-fold NOE had we not taken steps to avoid it. We were fortunately able to use internal metabolite signals as chemical shift references. For example, in samples containing obvious NMR signals from triacylglycerols, the $(-CH2-)_n$ resonance from the 27 carbons coresonating at the position of the fatty acyl chain at 30.5 ppm could be used as an environmentally insensitive shift reference. In samples without obvious lipid signals, the inositol resonances at 71.9 and 73.1 ppm served as an environmentally insensitive shift reference. The detailed assignments for the *in vitro* natural abundance ^{13}C NMR spectrum of the rat ventral prostate are shown in Table 2 where it can be seen that every resonance from every carbon in each metabolite can be observed. This illustrates the advantage which ^{13}C NMR offers over other means for metabolite analysis; we can obtain concentration data from each carbon in a metabolite and therefore compute statistical properties of the metabolite analyses from a signal spectrum. For example, tyrosine contains carbon types which resonate at seven distinct and resolved frequencies so that we can not only obtain its concentration in the tissue, but we can additionally obtain the statistical reliability of the data in terms of the mean and variance of the concentration from each sample based on seven independent measurements from a single spectrum. Other analytical techniques, such as HPLC or amino acid analysis, only offer this possibility if one repeats the entire analysis seven times.

Measurement of the concentrations for each metabolite from the natural abundance ^{13}C NMR spectra of tissue samples requires attention to a number of details which differ from those used for other analytical techniques. The NMR data are acquired using signal averaging because the ^{13}C nuclear magnetization cannot be observed in a single scan. Therefore, the nuclear spins are repetitively excited, the time-dependent sample magnetization from the $(n+1)^{th}$ radiofrequency pulse is measured and the signals are coherently added to those from the previous n pulses. The nuclear magnetization returns to equilibrium with a time constant commonly referred to as or the spin-lattice relaxation time. This time is on the order of 150-2000 milliseconds for the carbons in most tissue metabolites, while the repetition time we used for the radiofrequency pulses was 340 ms. Therefore the metabolite resonances are partially saturated and this must be corrected for when concentrations are computed. The correction factor is derived from the equation relating the magnetization, M(t) to the repetition time, t:

$$M(t) = M_o(1 - e^{-t/T_1}) \quad => M_o = M(t)/(1 - e^{-t/T_1})$$

The spin-lattice relaxation time, T_1, is easily measured using ^{13}C NMR, so that this correction can be applied to each resonance. Another factor which needs to be measured in order to correct the data is the nuclear Overhauser enhancement, η:

$$\eta + 1 = 1 + \gamma_H/2\gamma_C,$$

where γ is the nuclear gyromagnetic ratio. The NOE varies according to the rotational correlation time for the nucleus, τ_C, but for small molecules with $\tau_C < 10^{-9}$ sec, $\eta = 2.998$. The NOE is this large only for protonated carbons; non-protonated carbons do not acquire an NOE. The actual value η of is easily measured from the integral ratio of signals taken by acquiring two spectra, one with proton-

decoupling, and one with decoupling only during signal acquisition. An approach which obviates the need for these detailed corrections, and the approach we indeed took, is to adjust the pulse repetition time and the pulse angle so that both of these correction factors take on a value close to 1. This pulse angle is called the Ernst angle after Richard Ernst who first calculated its effects on NMR signals. The metabolite signals were reduced to tissue concentrations (in moles/Kg) through the following equation:

$$[m] = I_m[s]/(W\eta I_s n_C(1 - e^{-t/T_1})),$$

where I_m (I_s) is the integral of the metabolite (standard) resonance, [s] is the concentration of the

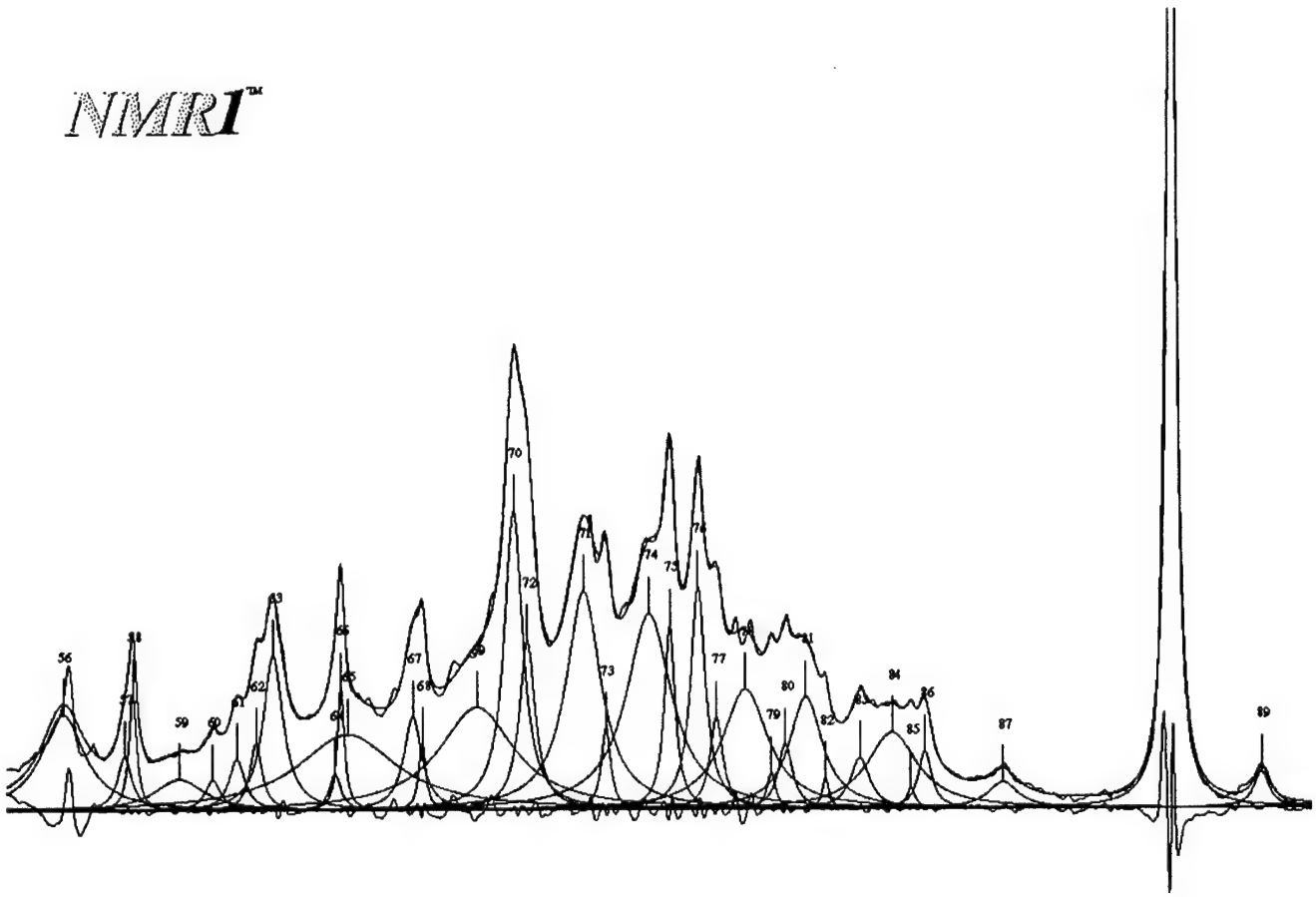

Figure 9. An example of non-linear least-squares curve-fitting of the aliphatic portion of the *in vitro* natural-abundance ^{13}C NMR spectrum of the rat normal ventral prostate.

standard, W is the tissue weight, η is the NOE, n_C is the number of coresonating carbons, and the exponential is the saturation correction factor. The resonance integrals were obtained through non-linear least-squares curve fitting using Lorentzian line shapes, as illustrated in Fig. 9. Here a convergence limit of 10^{-6} was used. It is clear from the fact that we observed 51 resonances from 27

metabolites that several metabolites often contributed to the integral of an observed resonance. We were able to account for each metabolite's contribution to a resonance using linear equations since we could observe almost all of the carbons from a given metabolite individually. The raw NMR data obtained are illustrated in Table 2. The first listing in Table 2 is from an unknown metabolite whose chemical shift (δ = 47.62 ppm) is indicative of a carbon directly bonded to a sulfur atom. There are additional NMR methods which can assist these more difficult assignment cases. In this instance a DEPT NMR spectrum showed that this resonance arose from a methylene carbon, so that its structural fragment was $-CH_2-S$, but its resonance position was distinct from taurine , a likely candidate molecule whose signals appear at δ = 48.41 and 36.17 ppm. We confirmed that this resonance did not arise from taurine by adding authentic taurine to the tissue sample and observing that the added taurine appeared as distinct resonances, separate from the unknown signal.

Table 2 shows that we observe a number of amino acids, and citrate in the normal rat ventral prostate. The complete analysis of metabolites, including their concentrations (assuming 80 % water content) is shown in Table 3. In addition to all of the amino acids, except tryptophan, we observe NMR signals from inositol, lactate, glycogen, creatine, citrate, and triacylglycerols. It is important to note that we do not observe taurine signals in the normal prostate. The observed weak signals from triacylglycerols are likely to represent not prostate tissue, but residual surrounding adipose tissue which is difficult to completely dissect away from the prostate parenchyma in the diffuse ventral prostate of the rat. The concentrations of several metabolites are of interest. For example, the concentration of citrate (4.7 ± 1.5 mM) is much higher than that observed in any other tissue in the rat. The citrate concentration in the liver is less than 100 μM. This reflects the known special role of citrate in prostatic physiology and biochemistry as a chelator of zinc in seminal plasma. The presence of glycogen likely reflects the storage form of glucose sequestered within the smooth muscle cells in the prostate. Lactate is a normal constituent of semen, but some lactate in harvested tissue could represent post-agonal glycolysis of glycogen in the tissue after harvesting, but prior to freezing. Creatine perhaps also residues in the prostatic smooth muscle cells. The final non-amino acid metabolite of interest is inositol, whose function in the prostate secretions is unknown, but is a common component of seminal plasma. In man, inositol is found at a concentration of 3.3 mM in seminal plasma, while we find a slightly higher concentration of inositol (19.2 ± 8.4 mM) in the rat normal ventral prostate. The types and concentrations of amino acids (~ 8mM) found in the rat normal ventral prostate are typical for organs which perform considerable protein synthesis. The prostate

Table 2. Rat Normal Ventral Prostate ^{13}C NMR data.

Compound Name	Standard δ(ppm)	RVP δ(ppm)	Integral	Linewidth (Hz)
???????		47.62	1.73E+08	197
Ala	**16.8**	**16.78**	1.22E+08	142
Ala	**51.1**	**51.12**		86.26
Ala	**176.3**	**176.38**	1.79E+07	40.54
Arg	24.4	24.59	2.68E+08	57.05
Arg	28	28	1.81E+08	128.34
Arg	41	41.18	5.32E+08	22.81
Arg	54.6	54.46	8.52E+08	168
Arg	157	157.63	2.74E+07	50.03
Arg	174.7	174.57	4.60E+08	356
Asn	36.5	36.17	1.25E+08	348.71
Asn	52.6	52.33		
Asn	174.2	174.02		

Asn	174.5	174.57	4.60E+08	356
Asp	37.1	37.19	3.86E+08	50.57
Asp	52.7	52.82		
Asp	175	175.26	9.54E+07	74.64
Asp	178.3	178.26	1.16E+08	126.5
Citrate	45.17	45.17	2.48E+08	57.91
Citrate	75.49	74.98		
Citrate	178.85	179.32	3.55E+07	50.06
Citrate	181.63	182.01	4.37E+07	45.08
Creatine	37.19	37.18	3.81E+08	50.57
Creatine	54.11	54.03		
Creatine	157.47	157.31	2.27E+07	35.04
Creatine	174.93	174.53	4.60E+08	356
Cys	26	26.3	2.82E+08	40.51
Cys	57.3	56.95	1.51E+08	71.6
Cys	174.2	174.02		
Gln	28.3	28	4.65E+08	128.34
Gln	33	32.9	7.63E+08	42.81
Gln	55.2	55.18	8.52E+08	169
Gln	175.5	175.26	9.54E+07	74.64
Gln	179.5	179.32	3.55E+07	50.06
Glu	27.6	27.62	1.42E+08	69.7
Glu	34	34.07	5.18E+08	108.99
Glu	55.2	55.18	8.52E+08	
Glu	175.1	175.26	9.54E+07	74.64
Glu	181.8	182.01	4.37E+07	45.08
Gly	42	42.32	2.43E+07	
Gly	173	173.08	2.09E+07	40.6
Glycogen	61.37	61.81	9.56E+08	343
Glycogen	71.96	71.74	2.14E+08	47
Glycogen	72.21	71.74	2.14E+08	47
Glycogen	73.96	73	3.51E+08	47
Glycogen	77.73	76.73	6.63E+08	47
Glycogen	100.48	100.27	2.11E+06	85
His	28.5	28	2.07E+08	128.34
His	55.3	55.18	8.52E+08	47
His	117.7	117.66	5.81E+07	76.4
His	131	131.34	4.61E+07	36.59
His	136.7	136.63	1.98E+08	262
His	174.4	174.53	4.60E+08	356
Ile	11.8	11.88	2.28E+08	214.47
Ile	15.4	15.36	9.60E+07	131.74
Ile	25.2	25.25	8.27E+08	145.24
Ile	36.6	36.49	1.02E+08	349
Ile	60.4	60.39		
Ile	174.7	174.57	4.60E+08	356
Inositol	71.91	71.76	2.06E+08	47.34
Inositol	73.1	73	3.36E+08	57.06
Inositol	73.29	73	3.36E+08	57.06
Inositol	75.13	75.25	6.63E+08	47

Lactate	**20.95**	**20.67**	2.45E+08	94.98
Lactate	**69.24**	**69.05**	3.69E+08	237.54
Lactate	**183.28**	**182.01**	4.37E+07	45.08
Leu	**21.6**	**21.48**	1.17E+08	57.56
Leu	**22.7**	**22.79**	1.44E+09	324
Leu	**24.9**	**24.59**	3.79E+08	62.21
Leu	**40.5**	**40.38**	2.31E+08	38.27
Leu	**54.2**	**54.03**		
Leu	**176.1**	**176.38**	1.73E+07	40.54
Lys	21.9	22.02	1.15E+09	240.3
Lys	26.7	26.3	3.19E+07	46.21
Lys	30.2	30.29	1.57E+09	137.48
Lys	39.5	39.77	5.61E+08	133.8
Lys	54.8	54.7	8.52E+08	47
Lys	174.9	174.53	4.60E+08	356
Met	**14.7**	**14.88**	3.38E+08	115.5
Met	**29.6**	**30.29**	1.87E+09	137.48
Met	**30.5**	**30.56**	0.00E+00	
Met	**54.7**	**54.7**	8.52E+08	47
Met	**174.8**	**174.57**	4.60E+08	356
Phe	**37**	**37.19**	3.20E+08	50.57
Phe	**56.8**	**56.71**	1.12E+08	71.6
Phe	**128.6**	**128.64**	3.14E+08	109.86
Phe	**130.3**	**130.29**	4.78E+08	118
Phe	**130.3**	**130.29**	4.78E+08	118
Phe	**136.2**	**135.87**	8.81E+05	10.58
Phe	**174.5**	**174.57**	4.60E+08	356
Pro	23.9	23.48	4.23E+08	82.05
Pro	29.2	30.29		
Pro	46	46.64		
Pro	61.1	61.04	1.20E+09	47
Pro	174.1	174.02		
Ser	56.9	56.93	1.51E+08	71.6
Ser	60.8	60.39	3.10E+08	117.3
Ser	172.6	172.47	8.27E+07	82.05
TAGs	**14.72**	**14.88**	3.38E+08	115.5
TAGs	**23.45**	**23.46**	4.23E+08	82.05
TAGs	**25.59**	**25.61**	8.27E+08	140.56
TAGs	**26.35**	**26.33**	3.19E+07	46.21
TAGs	**27.92**	**27.62**	1.24E+08	61.4
TAGs	**30.47**	**30.59**	1.86E+09	137.48
TAGs	**32.76**	**32.9**	4.23E+07	49.71
TAGs	**34.54**	**34.38**	5.10E+08	102.51
TAGs	**62.67**	**62.63**	1.20E+09	47
TAGs	**69.9**	**69.77**	3.69E+08	47
TAGs	**128.79**	**128.64**	3.14E+08	109.86
TAGs	**130.45**	**130.32**	4.78E+08	117.93
TAGs	**172.34**	**172.47**	8.27E+07	82.05
Taurine	36.17			
Taurine	48.41			

Thr	**20**	**20.09**	4.84E+08	86.07
Thr	**61**	**61.04**	3.10E+08	117
Thr	**66.6**	**66.58**	2.77E+08	43
Thr	**173.5**	**173.53**	2.09E+07	40.6
Tyr	**37**	**37.19**	3.81E+08	82.22
Tyr	**56.8**	**56.71**	1.19E+08	71.6
Tyr	**117**	**116.42**	4.62E+07	49.52
Tyr	**128**	**127.92**	4.52E+07	109.19
Tyr	**130**	**129.94**	1.75E+08	77.94
Tyr	**156**	**157.31**	2.27E+07	35.04
Tyr	**174.5**	**174.57**	4.60E+08	356
Val	**17.4**	**17.26**	3.12E+08	106.3
Val	**18.6**	**18.61**	2.90E+08	86.07
Val	**29.7**	**30.29**		
Val	**61.1**	**61.04**	3.10E+08	117.03
Val	**174.8**	**174.57**	4.60E+08	356
Acetonitrile	**5.445**	2.19E+09	2.19E+09	43.53
Acetonitrile	**121.687**	2.06E+09	2.06E+09	49.71

Table 3. Metabolites found in Rat normal Prostate and MLL Prostate Tumor.

Compound Name	Normal Average Conc (mM)	Normal Standard Deviation	Tumor Average Conc (mM)	Tumor Standard Deviation
Acetonitrile#	190.9	18.3	190.1	8.4
Ala	3.4	1.8	6.7	
Arg	5.4	2.5	4.0	
Asn*	4.7	2.0	-	-
Citrate*	4.7	1.5	1.2	1.0
Creatine	3.9	1.5	4.0	
Cys*	4.0	1.0	-	
Gln	4.9	2.1	5.5	
Glu*	5.5	1.5	9.3	2.2
Gly	4.1	1.7	6.5	
Glycogen*	2.7	1.8	-	-
His	4.6	1.6	6.4	2.0
Ile*	3.0	1.6	7.1	1.0
Inositol*	19.2	8.4	8.7	1.8
Lactate	5.9	2.7	4.1	1.0
Leu*	17.6	8.1	6.7	
Lys*	12.6	9.5	-	
Met	6.8	2.6	4.0	
Phe*	12.7	8.1	-	-
Pro*	16.1	12.6	-	-
Ser	7.2	2.7	7.1	
Triacylglycerols*	3.6	0.6	40.2	6.9
Taurine*	-	-	29.6	1.8
Thr	12.7	8.9	22.3	15.3
Tyr*	9.1	7.0	-	-
Val*	9.7	4.3	-	-

*Indicates that the difference between tumor and normal is significant ($P<0.05$).
#Acetonitrile was an external intensity reference contained in a sealed capillary.

produces enzymes, particularly kallikrein (prostate specific antigen) whose function in semen is to cleave semenogelin post-ejaculation so that semen can liquefy in the vagina and the sperm can become motile.

2.C.3. ***Metabolites found in a rat prostate tumor.*** We have obtained approximately 40 natural-abundance ^{13}C NMR spectra from samples of normal rat prostate tissues, and 3-6 specimens each of the tumors listed in Table 1. While a complete analysis of each of these spectra is beyond the scope of the present progress report, and is the subject of a current manuscript in preparation, we include the data for a representative sample, that of an MLL tumor which was androgen insensitive, poorly differentiated and metastatic to the lymph nodes and the lungs. The ^{13}C NMR spectrum of this tumor sample (Fig. 10) shows a markedly different pattern of signals from that found for the normal ventral prostate (Fig. 8). In particular, there is a barely detectable citrate signal at 45 ppm (peak 24), and the inositol signals near 73 ppm (peaks 9-11) are significantly attenuated. On the other hand, the signals from triacylglycerols, notably the methylene chain signal at 30.5 ppm

(peak 32 in Fig. 10), and from taurine (at 36.17 and 48.41 ppm; peaks 23 &29 in Fig. 10) are greatly enhanced. A quantitative comparison of the concentrations of the various metabolites between the normal ventral prostate and this MLL tumor sample is shown in Table 3 and reveals that many amino acid resonances are substantially reduced in the tumor. More important is the observation that citrate and inositol concentrations are 2-4 fold reduced in the tumor, while there is a 10-fold increase

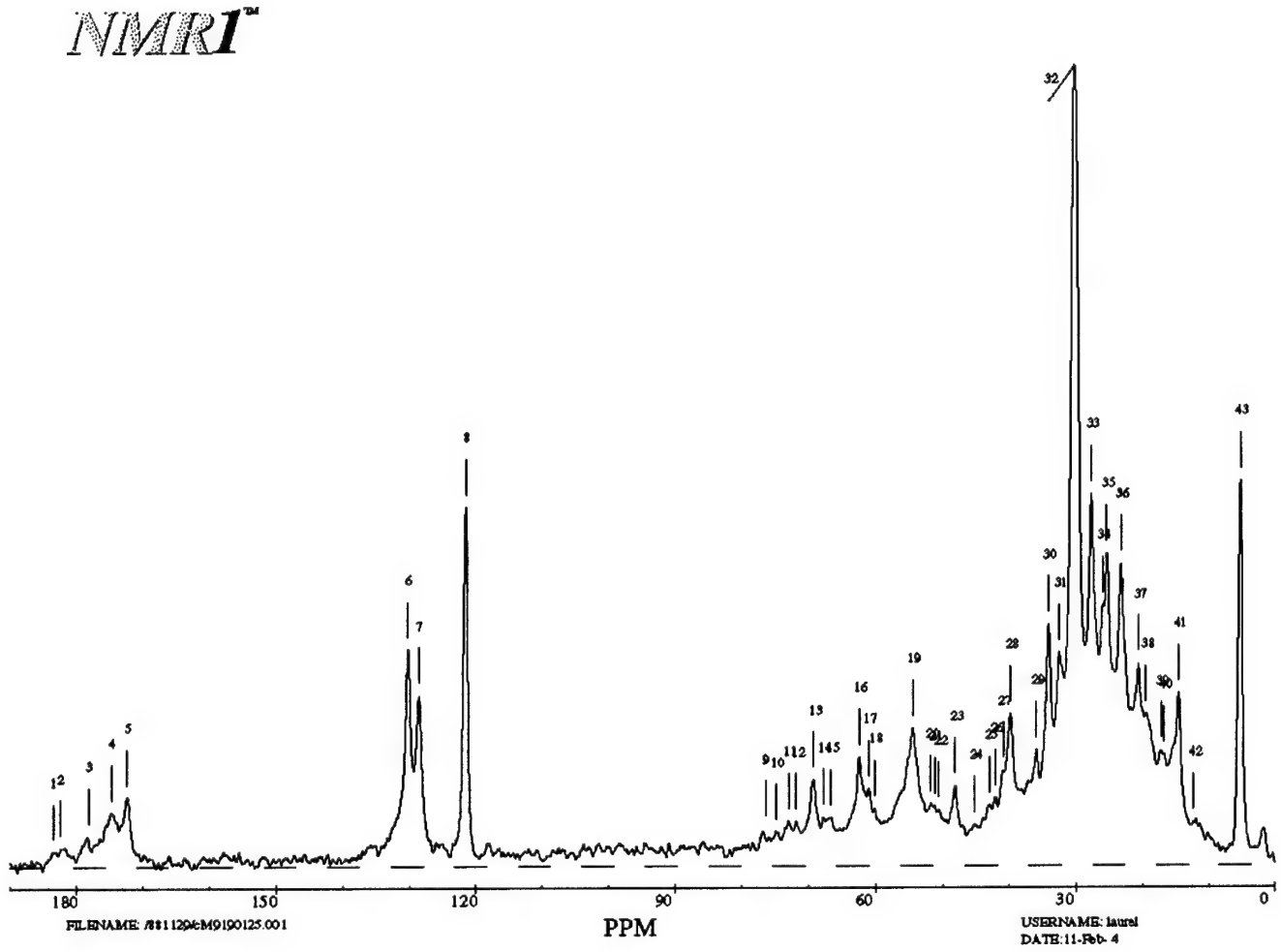

Figure 10 . Natural abundance ^{13}C NMR spectrum of a rat MLL prostate tumor with the following characteristics: Androgen insensitive, poorly-differentiated, metastatic to the lymph nodes and the lung. Signals numbered 8 and 43 are from the standard.

in lipids. No glycogen could be observed in the tumor , nor could alanine, asparagine, cysteine, lysine, phenylalanine, proline, tyrosine or valine (Fig. 11). The decrease in citrate indicates that *aconitase* is no longer inhibited in the tumor compared with its metabolism in the normal gland, and this is supported by the observation of a 2-fold increase in glutamate, which is synthesized from citrate after the *aconitase* step in the Kreb's cycle. The large increase in lipids is also in agreement with an altered citrate metabolism in which ATP-citrate-lyase must have been activated in the tumor

so that carbons from citrate now can flow into fatty acid synthesis and triacylglycerols. Several studies have reported increases in the gene expression of fatty acid synthetase as a sequel to tumorigenesis (Rossi *et al.*, 2003). Note also the presence of large amounts (~30 mM) of taurine in this androgen insensitive tumor (peak 23 in Fig. 10). The synthesis of taurine is under the control of

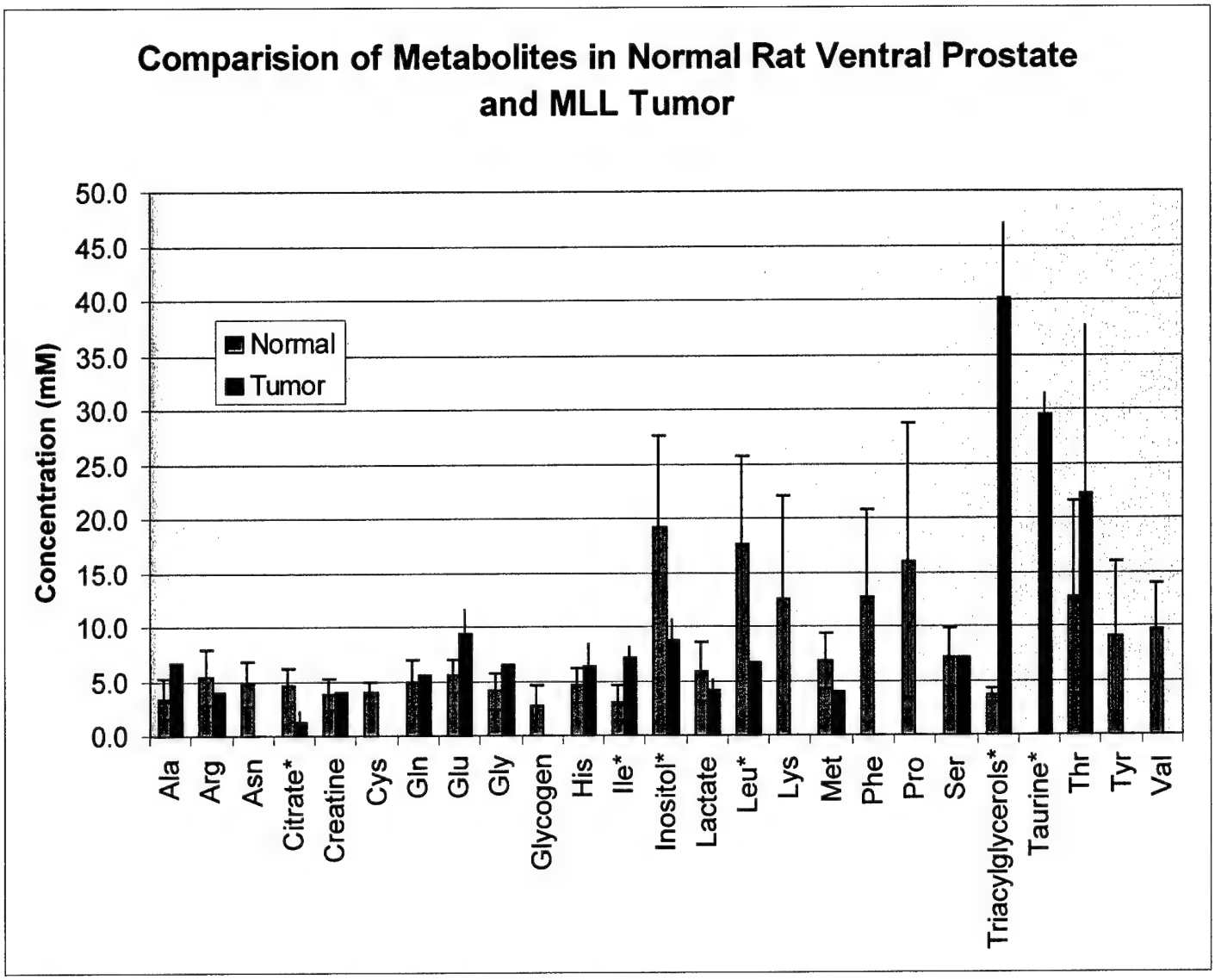

Figure 11. Comparison between the metabolites determined by means of natural abundance ^{13}C NMR spectroscopy in the rat normal ventral prostate (blue) and those from a metastatic MLL tumor (red), *in vitro*. Note the large differences observed for citrate, triacylglycerols, inositol, and several amino acids. Where known, the errors are shown based on the standard deviation of the data from more than one metabolite carbon resonance.

protein kinase Cε and Cornford *et al.*, 1999 have recently shown that this kinase is highly expressed in prostate cancer tissues.

2.C.5. Taurine as a marker for androgen-insensitive tumors. An analysis of the ^{13}C NMR spectra all of the Dunning rat prostate samples was performed. The results of primary interest are summarized in Table 4. *In vitro* natural abundance ^{13}C NMR spectroscopy of the described benign

and malignant Dunning prostatic tissues revealed prominent taurine peaks at 48 and 36 ppm, *in the androgen-insensitive* tissues, and *signals from tyrosine, at 37.1 ppm in the androgen-sensitive* tissues (Table 4). **Taurine** is present in millimolar amounts **only** in androgen-insensitive tumors, while **tyrosine** is detectable in **only** the androgen-sensitive tumors and both lobes of the normal prostate.

Table 4. ***Characteristics of Dunning Rat Prostatic Tissues and Tumor Types Examined with ^{13}C NMR Spectroscopy.***

Tissue or Tumor Type	Androgen Sensitivity	Degree of Differentiation	Metastatic Potential	Taurine μmol/g	Tyrosine μmol/g	Lactate μmol/g	Lipid μmol/g
Normal dorsolateral prostate	Yes	Well	None	0	13	8.5	0
Normal ventral prostate	Yes	Well	None	0	9.1	5.9	<3.6
G cell line	Yes	Poor	None	0	7.6	24.4	17
HI cell line	No	Well	None	16	0	10.8	7
AT-1 cell line	No	Poor	None	18	0	15.3	31
ML cell line	No	Poor	Yes	27	0	16.4	113
MLL cell line	No	Poor	Yes	30	0	4.1	40.2

Although the average amount of taurine is somewhat higher in the metastatic tumors analyzed, the values are not statistically different from those for the non-metastatic, androgen-insensitive tumors (HI, AT-1). The amount of tyrosine in the dorsolateral prostate is similar to that found in the androgen-sensitive G tumors, but it is less than the amount of tyrosine in the ventral prostate. The taurine elevation and tyrosine decrease in androgen-insensitive tumors mimic the pattern noted in normal rat prostate following castration (*Kochakian 1975; Kochakian 1974; Marvin and Awapara 1949*). The ability of these NMR data to distinguish androgen-insensitive from androgen-sensitive prostatic tissues is highly significant in light of the known influence of androgens on the taurine and amino acid metabolism of the prostate (*Kochakian 1974; 1975*).

Since taurine and tyrosine appear to be inversely related (*Halliday et al., 1988b*) in benign and malignant prostate tissues, we computed the taurine/tyrosine ratios for a variety of tissues examined. This ratio was estimated by signal to noise analysis to be <0.09 in the benign rat ventral prostate and 0.05 in benign human prostate tissue. These values jump to >35 in the rat MLL tumors and 15 in the malignant human prostate. Measurements of this ratio from published proton spectra of extracts from a primary human prostatic adenocarcinoma gave a value of 39, and a value of 103 from a DU145 androgen-insensitive, metastatic human tumor line (*Kurhanewicz et al., 1993*). Citrate is below natural-abundance ^{13}C NMR-detectable levels in our sample of Dunning rat tumors, while a substantial citrate resonance is seen in the normal prostate tissue. The most important of these findings from the Dunning rat model is the fact that taurine and tyrosine may act as a pair of NMR-detectable compounds that could be used to discriminate androgen-insensitive from androgen-sensitive tumors.

2.C.4. Quantitative Analysis of ^{13}C NMR spectra of Human normal prostate and tumors.

2.C.4.1 ***Human normal prostate.*** Samples of human prostate tissue were obtained from patients undergoing radical prostatectomy. These were flash frozen in liquid nitrogen and

subsequently thawed prior to examination by both ^{13}C NMR and histology. The ^{13}C NMR spectrum of histologically-normal human prostate tissue (Fig. 12) bears a close resemblance to that of the rat

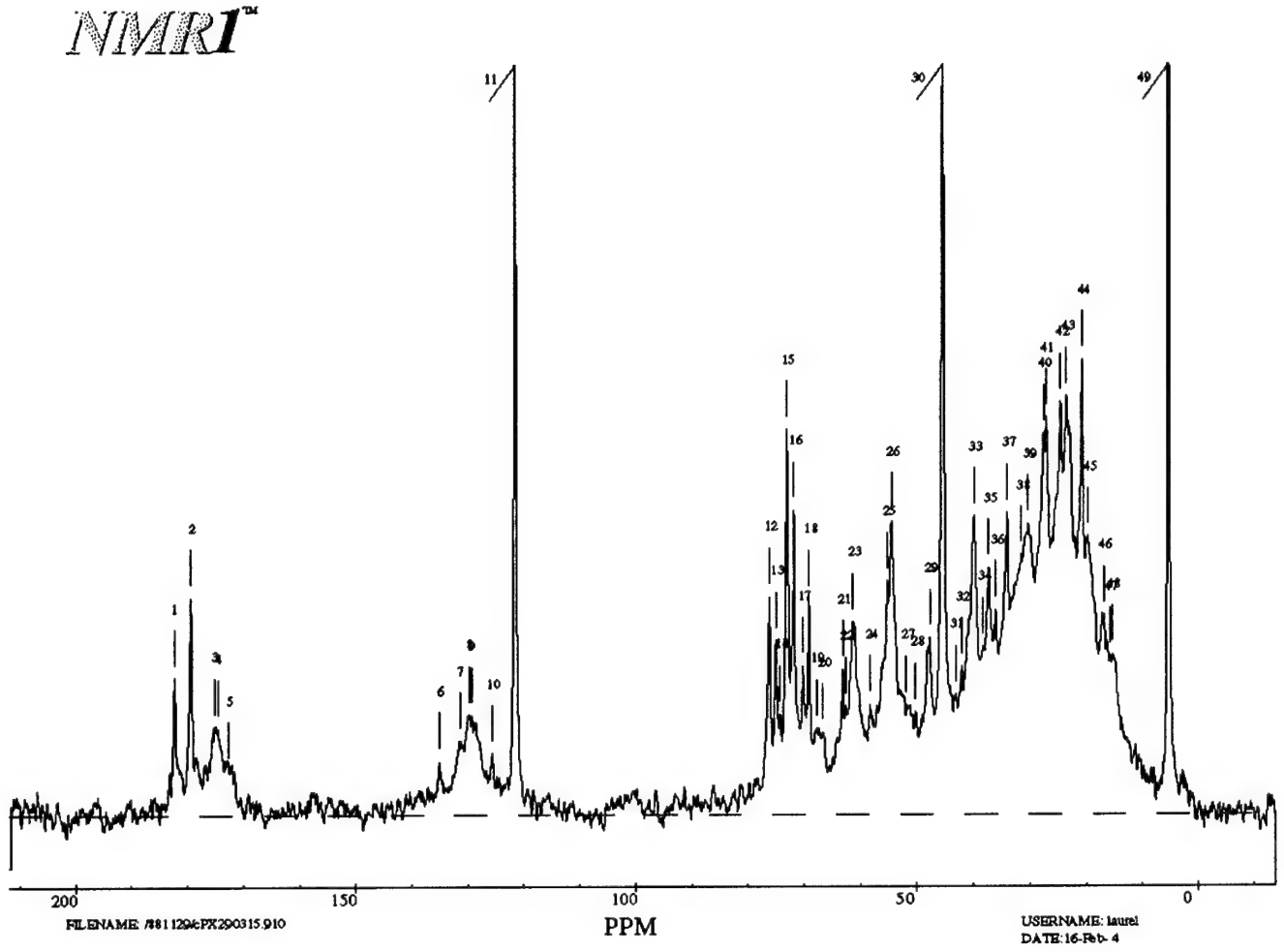

Figure 12. Natural abundance ^{13}C NMR spectrum of human non-malignant prostate tissue derived from a surgically-resected sample. Note the large citrate signal (peak 30) and the lack of triacylglycerol signals.

ventral prostate (Fig. 8). We note the very large citrate resonances in Fig. 12 at δ = 45 ppm (peak 30), δ = 75.5 ppm (peak 12), δ = 179 ppm (peak 2) and δ = 182 ppm (peak 1). Completely lacking are any signals from triacylglycerols; the most intense peak from these lipids would be found at 30.5 ppm, near peak 38 in Fig. 12. We do observe inositol (peaks 13, 15, 16), and many amino acids, including tyrosine (peaks 6 , 10 & 35 in Fig. 12). We used the same methods for measurement of the metabolite concentrations as described in detail above for the rat tissues to derive the data presented in Table 5. This particular non-malignant prostate sample contained 97 mM citrate, but no significant glycogen (δ ~ 100 ppm) and only 0.2 mM taurine. Other metabolites are found in amounts resembling those found for the rat normal ventral prostate above (Table 3).

Table 5. Metabolites found in Human Normal Prostate and Tumor.				
	Normal	Normal	Tumor	Tumor
Compound Name	Average Conc (mM)	Standard Deviation	Average Conc (mM)	Standard Deviation
Acetonitrile	190.0	9.6	203.0	15.6
Ala	3.2	0.5	4.0	4.5
Arg	4.1	2.2	9.5	3.3
Asn	3.7	1.3	7.8	-
Citrate*	96.6	4.1	9.9	1.4
Creatine	4.7	4.4	12.3	0.2
Cys	3.8	1.3	5.9	3.0
Gln	9.1	3.7	8.9	2.2
Glu	10.5	5.2	10.7	1.1
Gly	5.0	3.0	4.6	
Glycogen	0.0	-	0.0	-
His	7.5	3.6	7.7	0.1
Ile*	4.6	2.2	7.8	-
Inositol*	34.3	13.6	31.2	8.4
Lactate	15.0	10.3	27.5	0.7
Leu*	25.9	10.3	5.3	1.3
Lys	12.6	3.3	11.2	2.3
Met	10.7	2.9	13.2	-
Phe	4.8	0.8	10.6	2.5
Pro	3.8	1.7	7.0	1.2
Ser	4.8	1.9	0.0	-
Triacylglycerols*	0.0	-	40.6	2.1
Taurine*	0.2	0.0	11.8	0.7
Thr	4.9	0.8	8.7	0.4
Tyr	4.4	1.0	0.8	0.2
Val	15.8	5.6	11.9	1.1

*Indicates that the difference between tumor and normal is significant (P<0.05).

2.C.4.2 ***Human prostate tumor.*** An example of the natural-abundance ^{13}C NMR spectrum of a human prostate tumor tissue sample is shown in Fig. 13. Here we observe almost no citrate and a very large signal from triacylglycerols. Most of the observed NMR signals can be assigned to triacylglycerols. This tissue sample contained 11.8 mM taurine, 31.2 mM inositol and only 0.8 mM tyrosine (Table 5). A graphical comparison between the non-malignant prostate and prostate tumor is shown as Fig. 14 using the same arrangement of metabolites as seen previously for the rat data in Fig. 11. A comparison of Figures 11 and 14 shows that the human data closely follows that of the rat data. While there were some expected quantitative differences between these two species, in the main, it appears that the process of tumorigenesis involves several common pathways in both. In particular, the activation of citrate catabolism and the diversion of Kreb's cycle carbon flow into the synthesis of fatty acids for triacylglycerols is seen in both species tumors. This observation is directly in line with molecular biological investigations (Rossi et al., 2003) which have found that there is a

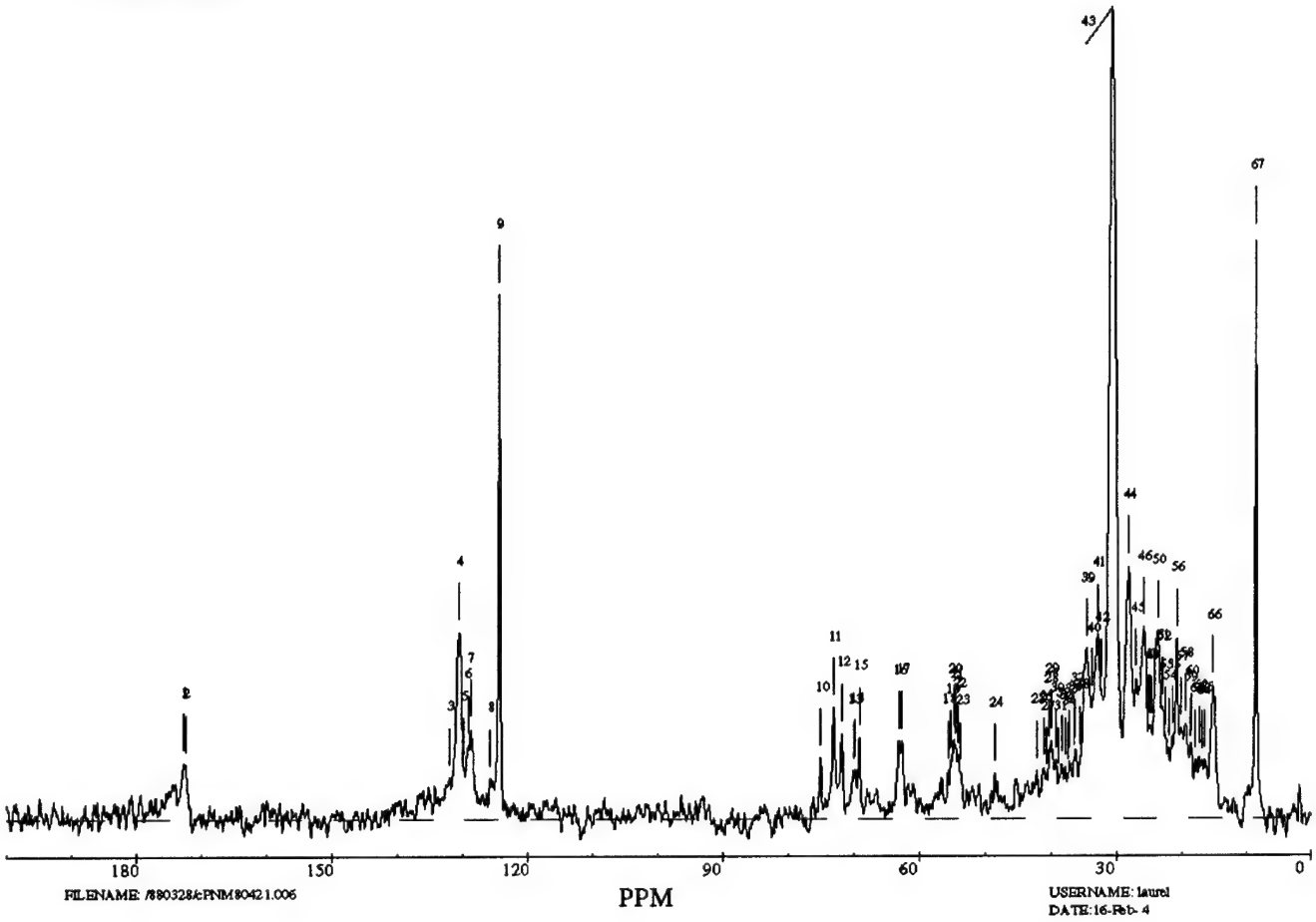

Figure 13. Natural-abundance ^{13}C NMR spectrum of a resected human prostate tumor, Gleason grade 8. Note the large signal from the triacylglycerol $(-CH_2-)_n$ methylenes at $\delta = 30.5$ ppm (peak 43) and the very weak citrate signal between peaks 24 & 25.

strong correlation between the expression levels of fatty acid synthetase and tumor grade in the human prostate. Once our entire data set from the large number of human samples is completely reduced in a similar manner, we will use computer-aided linear discriminant analysis (see below) to derive the most robust set of metabolic parameters which can be used to characterize tissue samples.

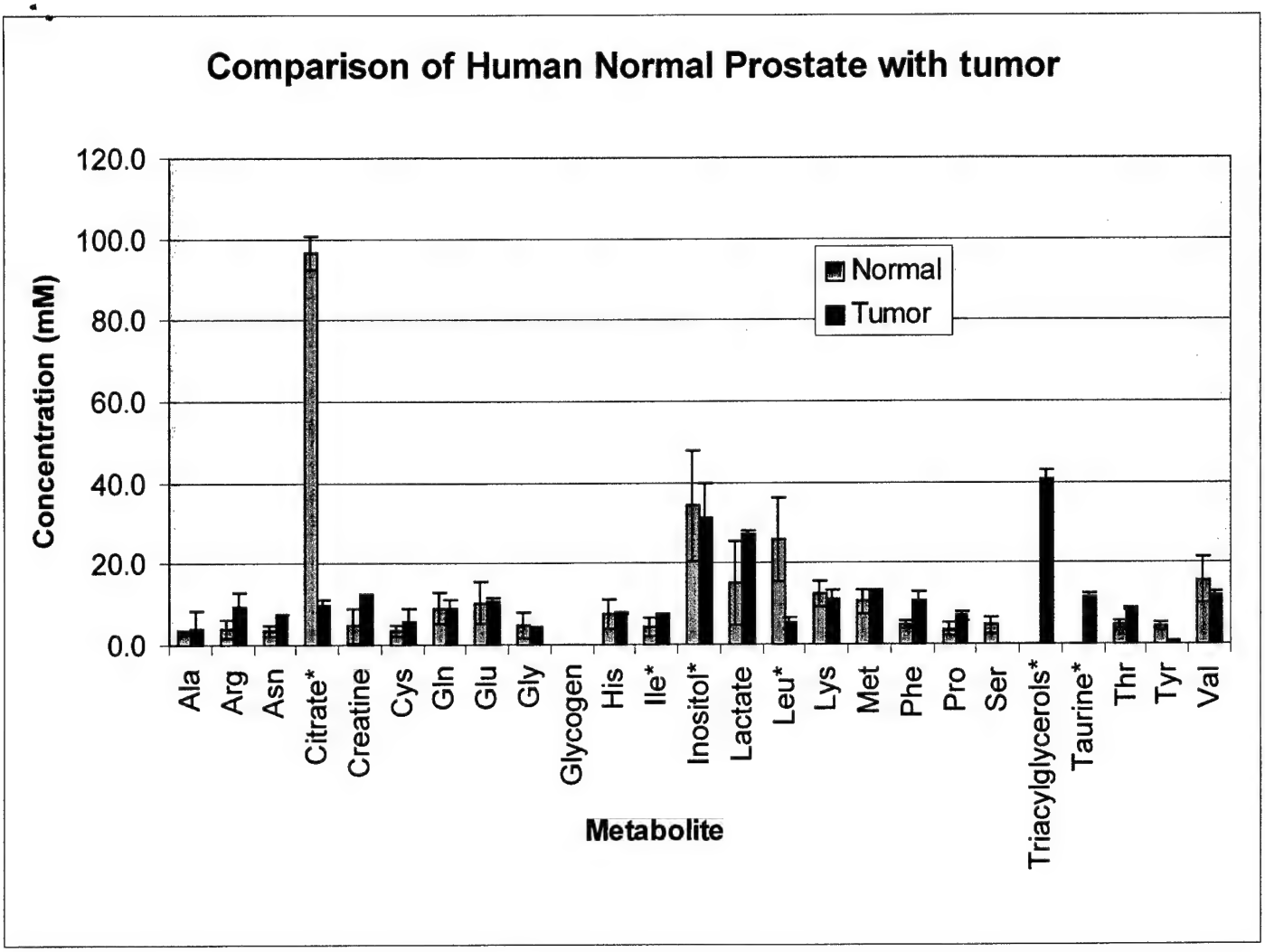

Figure 14. Quantitative comparision between the ^{13}C NMR spectroscopic data on metabolites derived from tissue samples of non-malignant and neoplastic human prostate.

C. Computer-based Linear Discriminant Analysis.

In order to utilize all of the information present in a ^{13}C NMR spectrum of prostate tissue, we have been working on the development of machine-learning techniques which could be applied in a clinical setting to distinguish NMR spectra from malignant and non-malignant prostate tissue samples. Our first approach is to use Linear Discriminant Analysis (LDA) to develop an empirical discrimination function based on the following types of data, the local amounts of prostate specific metabolites determined by NMR, optical and video histology of the tissue sections, Gleason score, PSA, PAP and special stains measurements, and the patient's progress, to determine the best linear discriminant predictors of tumor diagnosis, grade, and hormonal sensitivity based on the measurements. Clearly progress along these lines requires an investment in both computer hardware and software. We have purchased the commercial SAS package because it contains LDA code which we can begin to use for our analysis. The SAS software now runs on a Sun-Blade 1000 with dual 750 MHz cpus and 16 gigabytes of RAM. We are currently working on algorithms which will

automatically measure the ^{13}C NMR data and convert these measurements into a format compatible with SAS. Since this is a longer-term goal, we will report on our detailed progress in subsequent annual reports. Given the feedback from the LDA we will seek to refine our measurement of the predictors identified by the LDA in order to evaluate the potential for the developed empirical discrimination function for NMR to be used as a new diagnostic tool to predict tumor properties, with particular attention paid to androgen-sensitivity.

D. Application of non-invasive NMR spectroscopy in human patients.

^{1}H NMR Detection of citrate in prostatic tissue.

A representative high field (400 MHz) ^{1}H spectrum from benign human prostatic tissue (Fig. 15) shows the two doublets corresponding to citrate $H_{2,5}$ at δ = 2.6 ppm. Lactate appears at 1.3 ppm, and inositol appears at 3.6 ppm. The down-field region of the ^{1}H spectrum of this prostate tissue sample (not shown) displayed signals from aromatic protons, particularly from tyrosine at 6.9 and 7.2 ppm (*vide infra*) and phenylalanine. The metabolite lines in this spectrum are broadened by magnetic susceptibility variations from point to point within the tissue to a width of 23 Hz. These narrower resonances also ride on top of a broader baseline hump from the tissue and on the wings of the large residual water signal, even though the tissue sample was placed into a deuterated buffer, and the residual water signal was suppressed with gated proton decoupling. These results show that prostate metabolites, including citrate, are observable with proton NMR spectroscopy, in addition to that of ^{13}C NMR. Although we have applied ^{13}C NMR spectroscopy to human studies (Sillerud et al., 1988) we find that proton spectroscopy is technically less-demanding, and therefore more suited to initial clinical studies. We therefore turned to localized proton spectroscopy and imaging of the prostate in human cancer patients and in normal controls.

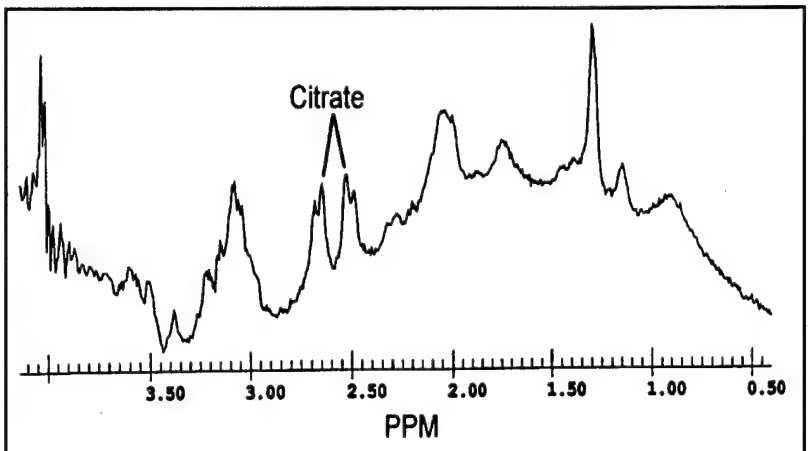

Figure 15. 400 MHz Proton NMR spectrum of 100 mg benign human prostate tissue.

NMR imaging of the prostate.

Proton NMR imaging and relaxation time measurements are able to provide important staging information relative to the extent of prostatic malignant disease, but are currently only able to differentiate between hyperplastic and malignant tissue on the basis of tissue contrast. No information is provided about the grade of the lesion. Prostate NMR imaging is generally well-established with several institutions using body-coil images and endorectal coils. Image-guided spectroscopy requires establishment of a high-quality image data set prior to the spectroscopic examination of the prostate. We have imaged several prostates of healthy male volunteers using a proton pelvic coil. We paid particular attention to how well the gland differs in contrast from surrounding tissue. Our results (using a T_2-weighted sequence [T_R=4 s, T_E=156 ms, 3 mm slice]) (Fig. 9) show both the central and the peripheral zones of the prostate. There is good discrimination

of the gland from the surrounding tissue, and from the adjacent seminal vesicles. The images show that we should be able to perform a three-dimensional reconstruction of the prostate upon which we can then superimpose our chemical shift imaging results.

Figure 16. Proton NMR images of the male pelvis. The **left** image is an axial section through the prostate taken with T_R=4 sec, T_E = 156 ms, thus giving T_2 weighting. Note the good differentiation of the prostate anatomy into the central and peripheral zones. Most tumors occur in the peripheral zone. The image on the **right** is from a coronal section through the prostate taken with the same acquisition parameters.

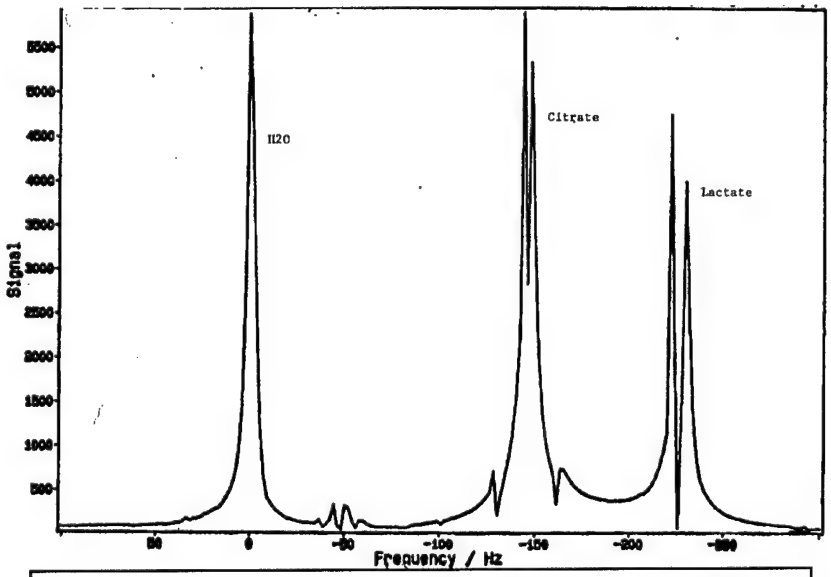

Figure 17. ^{1}H NMR spectrum of a phantom containing 0.5 M each of citrate and lactate in H_2O. This magnitude spectrum shows the 7 Hz splitting of the lactate methyl resonance, and the even smaller, 4 Hz splitting from the strongly-coupled citrate methylene protons. Note the excellent water suppression, where the 111 M water signal has been reduced to 0.5 M.

Detection of Citrate in phantoms in the GE Whole Body NMR system.

We have taken single-pulse spectra, using a 30 cm diameter head coil (and with the 15 cm double-Helmholtz pelvic coil), of a phantom (0.5 M citrate & 0.5 M lactate in H_2O) on the GE 1.5 T NMR system. The signal to noise ratio for a single pulse was found to be 72 ± 6 for the 4 methylene ($-CH_2-$) protons of citrate. The total line width for the citrate methylene protons was 6.9 Hz, and the width of the water signal was 4.3 Hz (Fig. 17). These results are indicative of the expected sensitivity and resolution to be obtained *in vivo*, and reflect the excellent progress that we have made shimming this system. These results are also typical of what other workers in the

field have obtained using similar phantoms, and in patients. We expect to obtain linewidths around 5-10 Hz in patients.

Development of Quantitative NMR Citrate Detection at 1.5 Tesla.

Progress in science always follows the evolution of observation methods from qualitative to quantitative; indeed, measurement connotes quantitation as well as observation. We therefore have sought to measure the actual concentrations of metabolites in the human prostate in vivo so that NMR spectroscopy could reach the diagnostic levels of current serum PSA measurements. In addition to the other factors which have already been discussed above with respect to the in vitro spectroscopy of the prostate tissue samples, there are unique considerations which come into play during NMR spectroscopy in human subjects. In order to measure, for example, citrate in the prostate, we need to have some means to calibrate the NMR spectroscopic response, to compensate for differences in subject positioning within the magnet, to accommodate changes in coil loading resulting from differences in body weight and composition, and to consider differences in linewidth arising from shimming variations and differences in magnetic susceptibility due to the adjacent, gas-filled rectum to the prostate. All of these features can be taken into consideration at the same time by using internal, water-based referencing, instead of the external, capillary-based referencing used for the in vitro tissue studies reported above. This procedure simply requires the acquisition of two data sets, one set with a small number of scans (typically 4-8) without any water suppression, and the other set with full water suppression with 128-256 scans. The unsuppressed spectrum is used to compute the unweighted signal to noise ratio for the prostate water signal. Now, since the noise in the spectrum is produced by mechanisms, like electrical noise in the receivers and amplifiers, and sample noise, which are independent of, and the same for, all of the above factors, we can use the noise as a reference. This is done by computing the signal to noise ratio for the metabolites and comparing that to the signal to noise ratio for unsuppressed water. One consideration here is a concern that the noise must be strictly random in order for this procedure to be robust. We tested this assumption by examining the characteristics of a signal-free noise region in a data set from a typical human subject. If the noise is indeed random, then it should have a Gaussian distribution with zero mean. The results of such a measurement (Fig. 18) show that the noise is indeed well-described by a random Gaussian function with zero mean, and width 34 units. The signal to noise ratio is defined as the signal height divided by the root-mean-squared noise, which in this case is the width of the noise distribution. The concentration of a metabolite, such as citrate, is then computed according to the following equation: $[\text{Citrate}] = (S_c C_w / n_H S_w)\ \text{SQRT}(N_w/N_c)$, where S_c is the signal to noise ratio for citrate, C_w is the concentration of water protons (1.1×10^5 mM), n_H is the number of protons ($n_H = 4$) contributing to the citrate signal, S_w is the signal to noise ratio for the unsuppressed water signal, N_w is the number of scans for the unsuppressed water data set, and

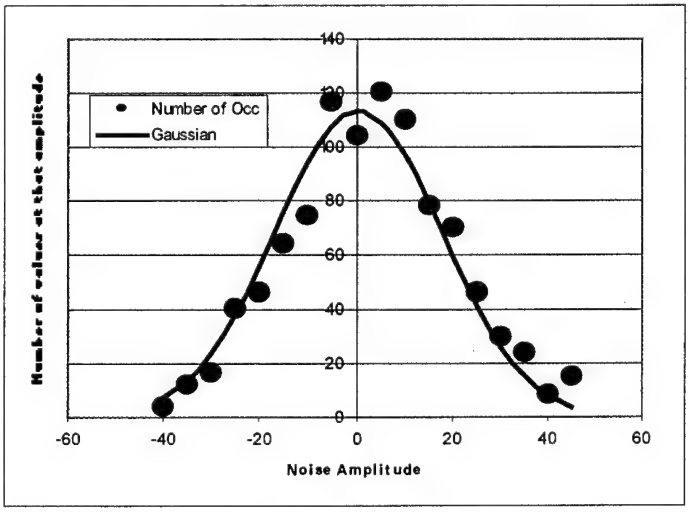

Figure 18. Measurement of the noise output from the NMR system with a human subject in the magnet. The noise (circles) amplitude has a mean value of 0.5 ± 17 units. The noise amplitude is well-described (solid line) by a Gaussian of width 34.

N_c is the number of scans for the water-suppressed metabolite spectrum. This procedure was extensively tested in phantoms containing 20 mM citrate, along with choline, lactate, glutamate and inositol. For example, we routinely achieve S_w = 7530, so that with S_c = 31.38, N_w = 8 and N_c = 256, one obtains a value of [Citrate] = 20.26 mM, which compares favorably with the actual concentration of citrate in the phantom of 20 mM. We removed and replaced the phantom for each of 28 measurements of the citrate concentration. The concentration of citrate was measured to be 19.6 ± 3.9 mM, which is in excellent agreement with the actual concentration of 20 mM. Note that there are no adjustable parameters in our method for the determination of metabolite concentrations; the method gives absolute values directly, without resort to any additional calibrations or standards. The distribution of the measurements is shown in Fig. 19. The standard deviation was 20% of the mean illustrating the expected accuracy which we should be able to attain *in vivo*. The measured signal to noise ratio of citrate also places an upper limit on prostatic citrate levels in the case of prostate tumors because we expect the citrate concentration to drop during tumorigenesis. The minimum detectable citrate is estimated from these phantom studies to be 31.38/20 ~ 2 mM. We already know from the *in vitro* tissue studies (*vide supra*) that citrate concentrations this low in humans (Table 5; Figs. 13 & 14) are overtly pathological and consistent with advanced cancer so that even knowing that the prostate citrate level in a human patient is below this detection limit would give significant information to the Urologist.

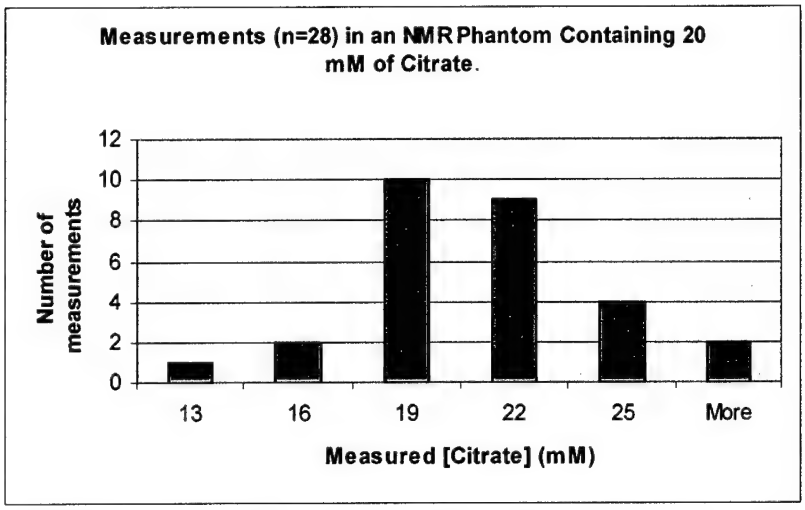

Figure 19. Measurement of the concentration of citrate in a phantom containing 20 mM citrate plus lacate, glutamate, inositol and choline. The mean [citrate] = 19.6 ± 3.9 mM.

In vivo ^{1}H detection of human prostatic citrate.

We have used both a proton pelvic coil and an endorectal coil (Medrad, Inc.) to detect prostatic metabolites *in vivo* in healthy male volunteers using the STEAM protocol. Fig. 20 shows the placement of the STEAM voxel onto the NMR image from a normal male volunteer. The volume of the voxel was 8 ml, and this encompassed both the central and the peripheral zones of the gland. We were able to place this voxel well away from the rectum, the bladder, and from periprostatic fat, which could interfere with lipid measurements.

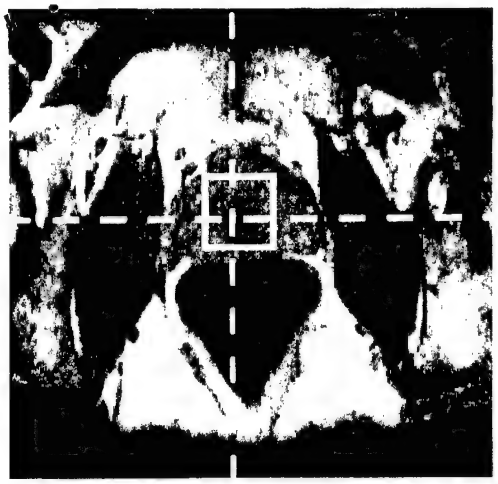

Figure 20. Placement of a STEAM voxel region of interest onto the prostate image of a normal male volunteer in order to obtain localized proton NMR spectra from this volume.

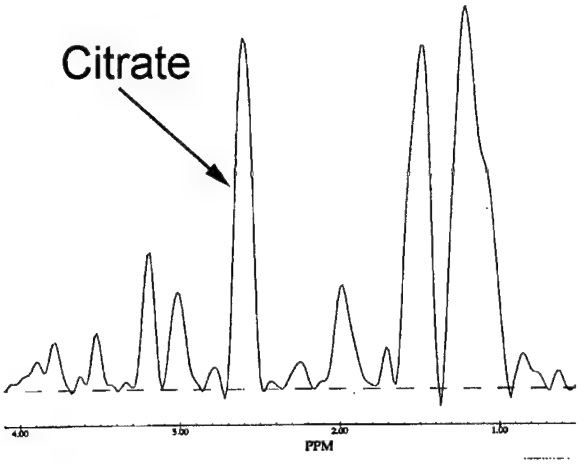

Figure 21. STEAM localized proton NMR spectrum at 1.5 Tesla of the prostate from a normal male volunteer. The citrate resonance is indicated at δ = 2.6 ppm.

The results from one such NMR spectroscopic exam (Fig. 12) show a signal at the characteristic chemical shift of citrate (δ = 2.6 ppm). Note that citrate resonates in a region of the spectrum which is relatively free from interference from other resonances. We also can observe nuclear resonances from choline (δ = 3.2 ppm), creatine (δ = 3.0 ppm), and glutamate (δ = 2.0 ppm). We anticipate the acquisition of even better proton spectra from humans *in vivo* as the localized spectroscopy program proceeds. The width of the citrate signal is 6.9 Hz, in agreement with our expectations (*vide supra*).

Quantitative Determination of Citrate concentrations in the human prostate *in vivo*.

With the development of quantitative methods for the determination of the prostatic concentration of citrate, we were interested in the application of this procedure to an initial control population of younger, disease-free men. We recruited 27 volunteers with an average age of 50 ± 7 years. To verify that these subjects represented a population without frank prostate cancer, we first measured the [PSA] and found a value of 0.9 ± 0.7, which is certainly well within the normal, tumor-free range (Fig. 22) of ≤ 4.0 ng/ml. These subjects were then examined by means of NMR imaging and STEAM spectroscopy. A STEAM voxel of total volume 4-8 ml was placed in the prostate and an NMR spectrum of the

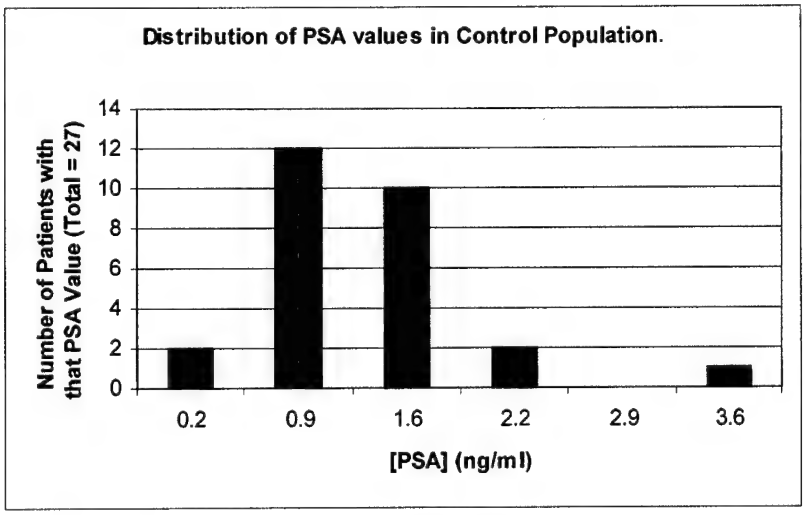

Figure 22. Distribution of PSA measurements in a control population of prostate disease-free 27 younger men (mean Age = 50 ± 7 years). The average [PSA] was found to be 0.9 ± 0.7 ng/ml.

gland was obtained using water suppression. A control spectrum was taken without water suppression in order to serve as an internal intensity reference. The concentration of citrate within the specified voxel was computed as indicated above, with the results shown in Fig. 23. We determined that the average citrate concentration in this subject population was 35 ± 15 mM. Three subjects had citrate concentrations of 66 mM or greater, while only one subject had a value below 20 mM (13.4 mM).

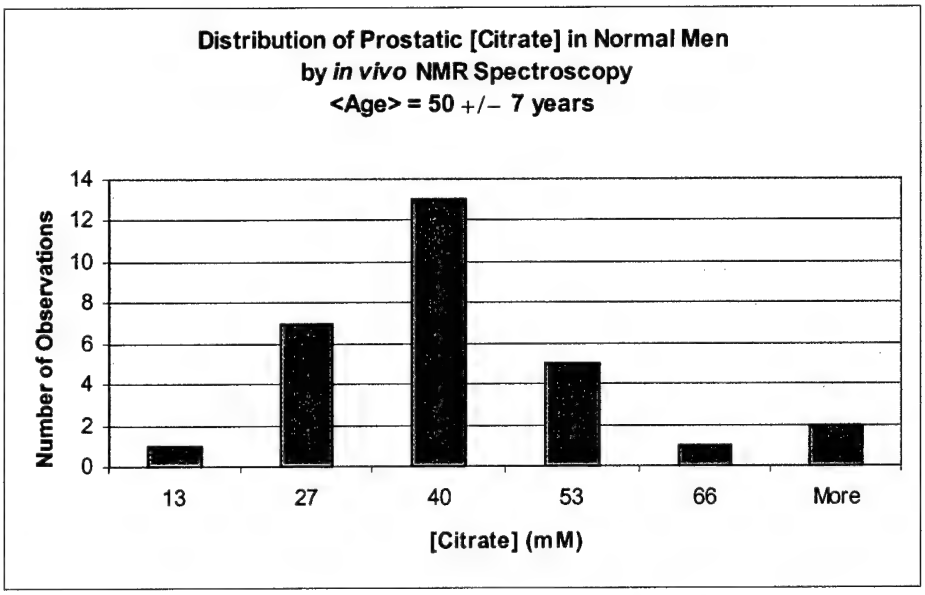

Figure 23. Distribution of the STEAM NMR-measured citrate concentration in the prostates of 27 normal male volunteers of average age 50 years.

Since we had measured the [PSA] and the [citrate] in each of these subjects, we were interested to know if there was any correlation between these measurements. We considered the existence of such a correlation highly unlikely, since the appearance of PSA in the blood is a pathological, rather than a normal process, whereas the prostate synthesizes citrate as part of its normal metabolic activity. The results (Fig. 24) show that there was indeed no detectable relationship between [citrate] and [PSA] in this control group. The least-squares line fitted to the data has a slope of 0.2 ± 4.4 (P > 0.95) which is statistically indistinguishable from a slope of zero. Identical results were obtained when the fit was performed by reversing the axes. We conclude that for younger men, who are free from prostate disease, there is no apparent coupling between the appearance of PSA in the serum and the amounts of citrate synthesized in the prostate.

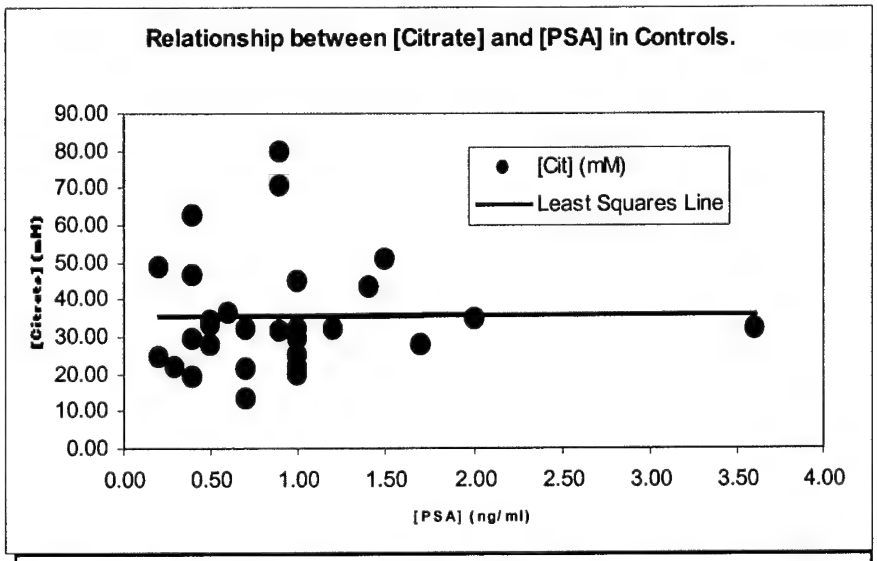

Figure 24. Relationship between the concentration of citrate and serum PSA measurements in a control group of 27 men of mean age 50 years.

Measurement of Prostatic [Citrate] in Patients.

Since the goal of this research is to develop better methods for the detection, diagnosis and prognostication of prostate disease, primarily prostate cancer, we were eager to apply the quantitative measurement procedures developed above to a patient population. In our Urology

practice, three types of patients were available for study in addition to our control group; those seeking a vasectomy, patients symptomatic for BPH (benign prostatic hyperplasia) and those with elevated serum [PSA] who are suspected of bearing frank tumors. We measured the serum [PSA] and conducted NMR STEAM spectroscopy and imaging on all of these subjects.

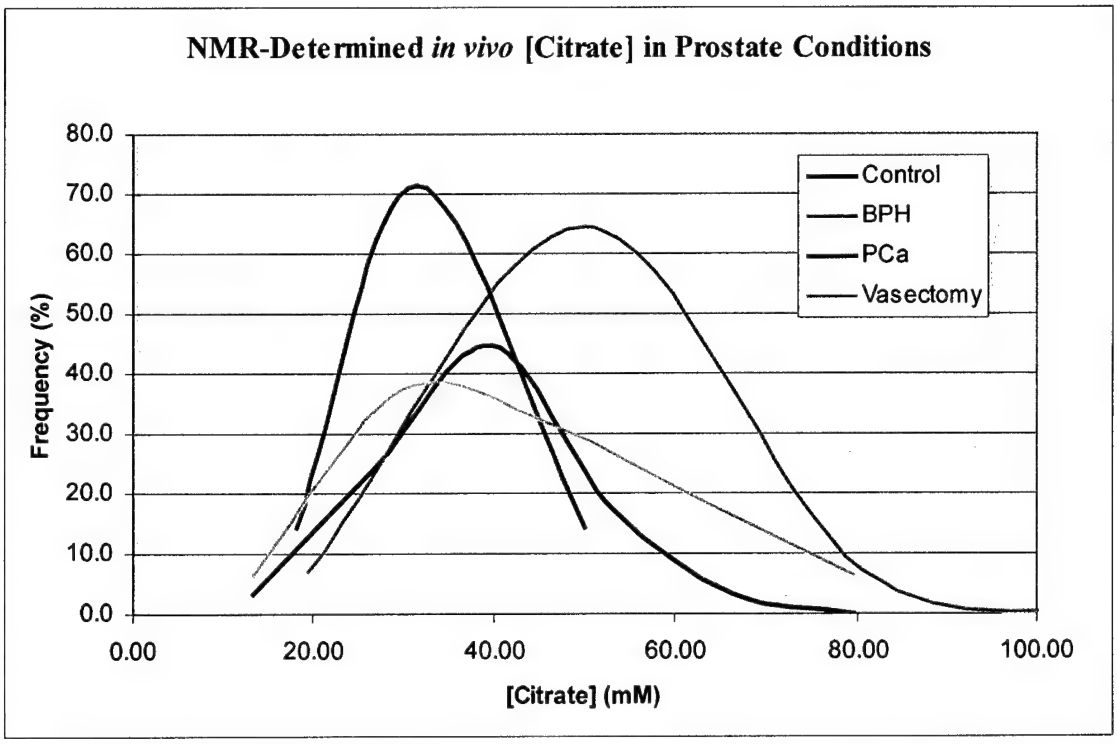

Figure 25. Distributions of the concentrations of citrate in the human prostates of four different study groups; a control group of 27 normal men (Control), a group of 14 BPH patients (BPH), a group of 16 vasectomy patients (Vasectomy) and 7 patients with prostate cancer (PCa).

Data on citrate for these four groups of patients are summarized in Fig. 25. The BPH group had the highest average [citrate] = 53 ± 27 mM, a value which is 150 % of the control group and significantly different from it ($P < 0.05$). The distribution curve for the vasectomy patients looks like a composite of the control and BPH groups. There was no statistical difference between the mean of the vasectomy group (32 ± 14 mM) and that of the control group (35 ± 15 mM); a not unexpected result. There was a significant difference between the mean citrate concentration in the prostate of the cancer group (28 ± 8 mM) with that of the control group and of the BPH group. Since prostate cancer almost always develops in older men, and these men are most prone to BPH, prostate cancer often develops against a background of BPH, so that our observation of a significant difference between the citrate concentrations in these two groups is what should be used to judge the applicability of these data in the clinic. Even though it is too early to make firm conclusions with respect a possible inverse relationship between [PSA] and [citrate] in the prostate, it is interesting to note that the lowest [citrate] in a cancer patient (18 mM) was observed in the subject who had the highest [PSA] (264 ng/ml). We are encouraged that [citrate] in the prostate appears to be a powerful discriminator with diagnostic potential for prostate cancer. However, we have seen from the *in vitro* tissue analyses, that the inclusion of measurements of additional metabolites will almost certainly improve the discrimination potential of NMR spectroscopy in prostate cancer diagnosis.

Key Research Accomplishments

1. The normal prostate contains modest amounts of epithelium; the average is 12.7 ± 5.9 % by area. Prostatic adenocarcinoma, on the other hand contains twice the epithelium at 25.3 ± 7.9 % by area.

2. All of the citrate in prostatic tissue is visible to NMR.

3. The NMR method provides accurate quantitation of tumor metabolites.

4. We can observe, natural-abundance ^{13}C NMR spectra from tissue samples obtained from residual human prostate tissue obtained during surgical resection of the gland. Signals from citrate carbons $C_{2,5}$ and lipid methylene carbons $(-CH_2-)_n$ were resolved well-enough so that measurements could be made of their respective intensities. Quantitative agreement was found between the citrate integrals (at δ = 47 ppm), relative to the standard, and the results of an enzymatic assay performed on the tissue after the NMR studies were completed.

5. Citrate amounts are higher and lipid amounts are lower in benign tissue in comparison to malignant tissue. The difference in normalized citrate peak intensity between benign and malignant human prostatic tissue was found to be statistically significant by Student's t-test for unequal variances ($p < 0.02$).

6. Comparison of the lipid methylene peak intensities from ^{13}C NMR spectra of human prostate tissue revealed that lipid differences between benign and malignant tissue values are even more significant ($p < 0.005$), and with less overlap, than the citrate differences.

7. There is a direct correlation between prostate epithelial area and citrate production in the benign samples. The slope of the linear fit to the data is significantly different from zero ($p < 0.001$). The results for the malignant prostate tumor samples show a weak inverse correlation between citrate and epithelial area.

8. High field (400 MHz) ^1H spectra from benign human prostatic tissue show signals from citrate $H_{2,5}$ at δ = 2.6 ppm. Lactate appears at 1.3 ppm, and inositol appears at 3.6 ppm. The down-field region of the ^1H spectrum of this prostate tissue sample displayed signals from aromatic protons, particularly from tyrosine at δ = 6.9 and 7.2 ppm and phenylalanine.

9. Prostate NMR imaging (using a T_2-weighted sequence [T_R=4 s, T_E=156 ms, 3 mm slice]) shows both the central and the peripheral zones of the prostate.

10. We have used both a proton pelvic coil and an endorectal coil (Medrad, Inc.) to detect prostatic metabolites *in vivo* in healthy male volunteers using the STEAM protocol. An NMR spectroscopic exam shows signals at the characteristic chemical shift of citrate (δ = 2.6 ppm) as well as choline (δ = 3.2 ppm), creatine (δ = 3.0 ppm), and glutamate (δ = 2.0 ppm).

Reportable outcomes

1. The normal prostate contains modest amounts of epithelium; the average is 12.7 ± 5.9 % by area. Prostatic adenocarcinoma, on the other hand contains twice the epithelium at 25.3 ± 7.9 % by area.

2. All of the citrate in prostatic tissue is visible to NMR.

3. The NMR method provides accurate quantitation of tumor metabolites.

4. We can observe, natural-abundance ^{13}C NMR spectra from tissue samples obtained from residual human prostate tissue obtained during surgical resection of the gland. Signals from citrate carbons $C_{2,5}$ and lipid methylene carbons $(-CH_2-)_n$ were resolved well-enough so that measurements could be made of their respective intensities. Quantitative agreement was found between the citrate integrals (at δ = 47 ppm), relative to the standard, and the results of an enzymatic assay performed on the tissue after the NMR studies were completed.

5. Citrate amounts are higher and lipid amounts are lower in benign tissue in comparison to malignant tissue. The difference in normalized citrate peak intensity between benign and malignant human prostatic tissue was found to be statistically significant by Student's t-test for unequal variances ($p < 0.02$).

6. Comparison of the lipid methylene peak intensities from ^{13}C NMR spectra of human prostate tissue revealed that lipid differences between benign and malignant tissue values are even more significant ($p < 0.005$), and with less overlap, than the citrate differences.

7. There is a direct correlation between prostate epithelial area and citrate production in the benign samples. The slope of the linear fit to the data is significantly different from zero ($p < 0.001$). The results for the malignant prostate tumor samples show a weak inverse correlation between citrate and epithelial area.

Conclusions

The normal prostate contains modest amounts of epithelium; the average is 12.7 ± 5.9 % by area. Prostatic adenocarcinoma, on the other hand contains twice the epithelium at 25.3 ± 7.9 % by area. All of the citrate in prostatic tissue is visible to NMR. The NMR method provides accurate quantitation of tumor metabolites. We can observe, natural-abundance ^{13}C NMR spectra from tissue samples obtained from residual human prostate tissue obtained during surgical resection of the gland. Signals from citrate carbons $C_{2,5}$ and lipid methylene carbons $(-CH_2-)_n$ were resolved well-enough so that measurements could be made of their respective intensities. Quantitative agreement was found between the citrate integrals (at δ = 47 ppm), relative to the standard, and the results of an enzymatic assay performed on the tissue after the NMR studies were completed. Citrate amounts are higher and lipid amounts are lower in benign tissue in comparison to malignant tissue. The difference in normalized citrate peak intensity between benign and malignant human prostatic tissue was found to be statistically significant by Student's t-test for unequal variances ($p < 0.02$). Comparison of the lipid methylene peak intensities from ^{13}C NMR spectra of human prostate tissue revealed that lipid differences between benign and malignant tissue values are even more significant ($p < 0.005$), and with less overlap, than the citrate differences. There is a direct correlation between prostate epithelial area and citrate production in the benign samples. The slope of the linear fit to the data is significantly different from zero ($p < 0.001$). The results for the malignant prostate tumor samples show a weak inverse correlation between citrate and epithelial area. High field (400 MHz) ^1H spectra from benign human prostatic tissue show signals from citrate $H_{2,5}$ at δ = 2.6 ppm. Lactate appears at 1.3 ppm, and inositol appears at 3.6 ppm. The down-field region of the ^1H spectrum of this prostate tissue sample displayed signals from aromatic protons, particularly from tyrosine at δ = 6.9 and 7.2 ppm and phenylalanine. Prostate NMR imaging (using a T_2-weighted sequence [T_R=4 s, T_E=156 ms, 3 mm slice]) shows both the central and the peripheral zones of the prostate. We have used both a proton pelvic coil and an endorectal coil (Medrad, Inc.) to detect prostatic metabolites *in vivo* in healthy male volunteers using the STEAM protocol. An NMR spectroscopic exam shows signals at the characteristic chemical shift of citrate (δ = 2.6 ppm) as well as choline (δ = 3.2 ppm), creatine (δ = 3.0 ppm), and glutamate (δ = 2.0 ppm). These results indicate that we have made significant progress with respect to our specific aims during the initial funding year of this project. We are now in a good position to pursue computer-fitting of the NMR spectra with the aim to incorporate this data into an LDA scheme for the determination of the most significant metabolic differences between normal and malignant prostates. Our *in vivo* program of application of this research to human patients is now on a firm foundation. We look forward to the next year of research with eager anticipation because we are replacing our aging GE 1.5 Tesla whole body NMR system with a state-of-the-art Siemens instrument. This new instrument will be able to acquire chemical shift images of metabolites in the prostate with superior resolution and sensitivity.

References

Sillerud LO, Halliday KR, Griffey RH, et al: (1988) In vivo ^{13}C spectroscopy of the human prostate. Magn. Reson. Med. **8**:224-230.

Claflin, AJ, McKinney, EC and Fletcher, MA. (1977) The Dunning R3327 prostate adenocarcinoma in the Fischer-Copenhagen F1 rat: a useful model for immunological studies. Oncology 34:105-109.

Cornford P, Evans J, Dodson A, Parsons K, Woolfenden A, Neoptolemos J, Foster CS. Protein kinase C isoenzyme patterns characteristically modulated in early prostate cancer. Am J Pathol. 1999 Jan;154(1):137-44.

Dunning WF. (1963) Prostate cancer in the rat. Natl. Cancer Inst. Monogr. 12:351-369.

L. O. SILLERUD, C. H. Han, M. W. Bitensky, and A. A. Francendese "Metabolism and Structure of Triacylglycerols in Rat Epididymal Fat Pad Adipocytes Determined by ^{13}C Nuclear Magnetic Resonance" *Journal of Biological Chemistry* **261**(1986)4380-4388.

L. O. SILLERUD, and R. G. Shulman "Structure and Metabolism of Mammalian Liver Glycogen Monitored by ^{13}C Nuclear Magnetic Resonance" *Biochemistry* **22**(1983)1087-1094.

C. H. Han and L. O. SILLERUD "Synthesis of [guanidino-^{13}C]-Creatine and Measurement of the Creatine Phosphokinase Reaction in vitro by ^{13}C NMR Spectroscopy" *Magnetic Resonance in Medicine* **3**(1986)626-634.

Hall M, Silverman L, Wenger AS and Mickey DD. (1985) Oncodevelopmental enzymes of the Dunning rat prostatic adenocarcinoma. Cancer Res. **45:** 4053-4059.

Mickey DD, Stone KR, Wunderli H, Mickey GH, Vollmer RT and Paulson DF. (1977) Heterotransplantation of a human prostatic adenocarcinoma cell line in nude mice. Cancer Res. **37:**4049-4058.

Marvin HN, Awapara J: (1949) Effect of androgen on concentration of certain amino acids in the rat prostate. Proc. Soc. Exptl. Biol. Med. **72:**93-95.

Furuya Y, Akimoto S, Yasuda K, and Ito H. (1997) Apoptosis of androgen-independent prostate cell line induced by inhibition of fatty acid synthesis. Anticancer Research **17**:4589-4593.

Kochakian CD. (1973) Hypotaurine: Regulation of production in seminal vesicles and prostate of the guinea pig by testosterone. Nature **241**:202-203.

Kochakian CD. (1974) Free amino acid concentration of accessory sex organs of the rat: regulation by androgen. Fed. Proc. **33**:28.

Kochakian CD. (1975) Free amino acids of sex organs of the mouse: Regulation by androgen. Am. J. Physiol. **228**:1231-1235.

Kurhanewicz J, Dahiya R, Macdonald JM, Chang LH, James TL, Narayan P. (1993) Citrate alterations in primary and metastatic human prostatic adenocarcinomas: 1H magnetic resonance spectroscopy and biochemical study. Magn Reson Med **29**:149-157.

Marvin HN, Awapara J: (1949) Effect of androgen on concentration of certain amino acids in the rat prostate. Proc. Soc. Exptl. Biol. Med. **72:**93-95.

Wright CE, Tallan HH, Lin YY. (1986) Taurine: Biological Update. Ann. Rev. Biochem. **55**:427-453.

Rossi S, Graner E, Febbo P, Weinstein L, Bhattacharya N, Onody T, Bubley G, Balk S, Loda M. Fatty acid synthase expression defines distinct molecular signatures in prostate cancer. Mol Cancer Res. 2003 Aug;1(10):707-15.

Appendices: none